CHAPTER 7

Model Simulations of Global Tropospheric Ozone

Lead Author:
F. Stordal

Co-authors:
R.G. Derwent
I.S.A. Isaksen
D. Jacob
M. Kanakidou
J.A. Logan
M.J. Prather

Contributors:
T. Berntsen
G.P. Brasseur
P.J. Crutzen
J.S. Fuglestvedt
D.A. Hauglustaine
C.E. Johnson
K.S. Law
J. Lelieveld
J. Richardson
M. Roemer
A. Strand
D.J. Wuebbles

CHAPTER 7

MODEL SIMULATIONS OF GLOBAL TROPOSPHERIC OZONE

Contents

SCIENTIFIC SUMMARY

Simulations of chemical tracers and comparison with observations indicate that global three-dimensional (3-D) models are able to describe gross features of atmospheric transport, such as boundary layer ventilation and long-range transport from continents to oceans. The broad distributions of the tropospheric ozone, such as altitudinal and seasonal variation, are captured to within about a factor 2. Important inaccuracies still remain: stratospheric/tropospheric exchange, natural emissions of precursors (*e.g.,* NO_x from lightning), reactions in aerosols and clouds, and representation of processes not resolved at the scale of models.

Three-dimensional simulations of O_3 over polluted continents have shown some success in reproducing observed distributions of ozone, NO_x, NO_y, and hydrocarbons under conditions where emissions and meteorology are well characterized.

Models and analyses of observations show evidence for a large anthropogenic contribution to tropospheric ozone in the Northern Hemisphere (NH). A few global model studies report that tropospheric ozone has increased by more than 50% since pre-industrial times over large regions of the NH lower and middle troposphere.

The global mean hydroxyl radical (OH) concentrations predicted by a variety of 2-D and 3-D models are within a factor 1.3 of the values that have been derived from budget studies of methyl chloroform (CH_3CCl_3) and hydrochlorofluorocarbons (HCFCs), and are also consistent with analysis of ^{14}CO.

Two model intercomparison exercises have been conducted to test the ability of models to simulate a) the transport of short-lived tracers and b) basic features of O_3 photochemistry. More than twenty models participated. A high degree of consistency was found in the global transport of a short-lived tracer within the 3-D chemistry transport models (CTMs). General agreement was also found in the computation of photochemical rates affecting tropospheric O_3. These are the first extensive intercomparisons of global tropospheric models.

2-D tropospheric chemistry models capture the coarse features of the ozone distribution and are useful for some analyses. Quantitative assessments based on these models will remain highly uncertain. The model intercomparison cited above showed that 2-D models cannot transport short-lived species in the same manner or magnitude as 3-D models.

A set of five 2-D and 3-D models predicted the O_3 change expected for a 20% increase in methane (CH_4) concentration. All models predicted small tropospheric O_3 increases, ranging from 0.5 to 2.5 ppb in the tropics and the midlatitude northern summer. The large range in the results demonstrates the large uncertainty in quantitative assessment. All models predicted an increase in the effective CH_4 lifetime.

These simulations and a theoretical analysis of the tropospheric chemical system coupling CH_4, CO, and OH have shown that CH_4 perturbations decay with a lengthened time scale, about 13.6 (11.3-16.0) yr, as compared with the lifetime derived from total abundance and losses, about 9.4 yr. This longer residence time describes the decay of any reasonably sized methane pulse, including all associated perturbations to tropospheric O_3 and stratospheric H_2O. It also increases our estimate of the greenhouse effectiveness of CH_4 emissions by a factor 1.45 as compared with previous assessments.

7.1 INTRODUCTION

Tropospheric models contain mathematical formulations of the life cycles of the major tropospheric source gases and the photochemistry, transport, and surface exchange processes that couple them together and to the life cycle of tropospheric ozone. They are used to quantify the importance of the various terms in the life cycles and budgets for ozone as well as for methane and other ozone precursors. They allow an estimation of the concentration distribution of the main tropospheric oxidant, the hydroxyl (OH) radical in the troposphere, and of the processes by which it is controlled. The strong chemical tie between ozone and several other climate gases causes tropospheric ozone to be very important in the regulation of the Earth's climate. This indirect climatic role of ozone comes in addition to the direct climate effect of ozone due to its radiative properties.

The processes governing the tropospheric ozone budget are described in Chapter 5 and summarized in Figure 7-1. A substantial amount of the tropospheric ozone is produced in the stratosphere and transported to the troposphere at high and middle latitudes. The *in situ* photochemical production is several times larger than the import from the stratosphere, but is to a large extent counteracted by chemical loss. The relative importance of these processes to the ozone budget remains a topic for future research. In the boundary layer, ozone is deposited at the surface and produced on urban and regional scales that are not adequately resolved in global models. Transport processes, especially vertical transport of O_3 and its shorter-lived precursors such as NO_x (=NO+NO_2) and non-methane hydrocarbons (NMHC), affect tropospheric chemistry and determine the level of change in O_3 concentration in the upper troposphere, thereby strongly influencing the global budget of tropospheric ozone.

The development of our understanding of the tropospheric chemistry of ozone has been driven forward
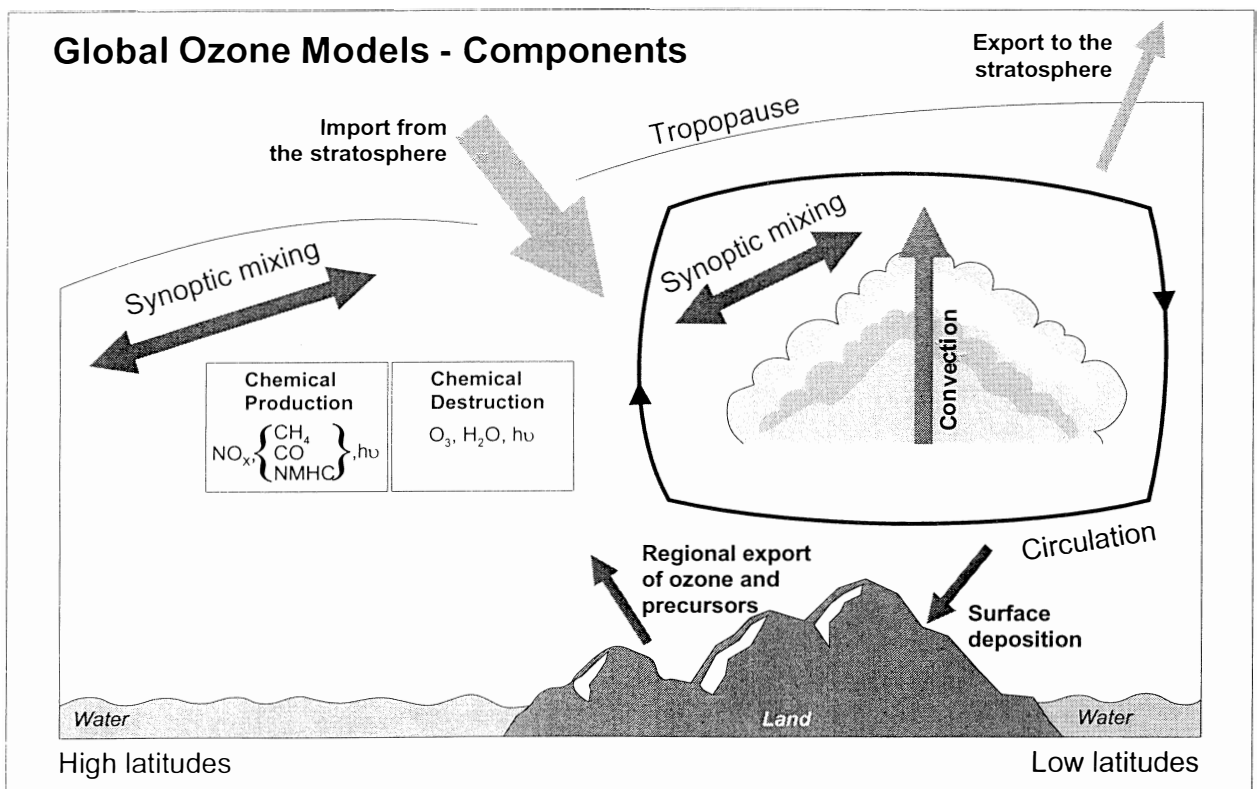

Figure 7-1. Processes governing the global tropospheric ozone budget. The major components are import of ozone from the stratosphere, chemical production and loss, deposition at the ground, and ozone production on the smaller urban and regional scales.

by a combination of careful field observation, laboratory investigation, and theoretical modeling. Modeling may point to hitherto undiscovered relationships between trace gases and processes, and observations can challenge our theoretical understanding, leading to the development of a more complete explanation of atmospheric systems.

Recently, theoretical modeling has been given heightened importance, particularly for ozone, through its role in explaining the relationship between atmospheric composition and the emissions of trace gases from human activities. Theoretical modeling offers the prospect of being able to unravel the cause of the trends and the possible role of human activities in them. This naturally leads to an important question as to whether any of these observed trends will continue in the foreseeable future. Furthermore, models offer the possibility to estimate future changes in ozone resulting from changes in emissions of ozone precursors.

Whether any of the conclusions derived from models concerning trends in ozone concentrations actually describe what happens in the real atmosphere depends on the adequacy and completeness of their formulation, which is tied to our understanding of physical and chemical processes in the troposphere, as well as on the accuracy of their input data. Testing of models involves comparison with observations, which are inevitably limited in their accuracy and coverage in space or time. In a complex model, it is difficult to explain the good agreement with observations often found in some atmospheric regions for some species and the rather poorer agreement sometimes found elsewhere. Tropospheric models are in their infancy at present; the global data sets required to validate them adequately are not yet available, nor is the computer capacity to handle all the processes that are believed to be important.

This chapter briefly surveys, in Section 7.2, the successes and problems revealed in recent 3-D model simulations of transport and chemistry in the troposphere. Most attention has been devoted to global models. In order to successfully model troposphere ozone globally, it is necessary to describe regional ozone, since the global picture is only a conjunction of regional parts. A few recent continental-scale model studies are therefore also assessed in Section 7.2.

A range of global-scale models have been used for studies of tropospheric ozone. Section 7.3 presents a short compilation of such 2-D and 3-D models. The section compares the zonally averaged ozone distribution and budget terms for stratosphere/troposphere exchange fluxes, chemical production and loss, and surface deposition in several of the models currently used for global ozone studies. A survey of the major limitations in current models is also included in Section 7.3, whereas Section 7.4 presents global model integration of some selected applications of key relevance for past, current, and future tropospheric ozone.

As a part of the IPCC (1994) assessment as well as this assessment (Section 7.5), a comparison of global chemical models, that were used to calculate the effects of changes in methane (CH_4) on chemistry and climate forcing, was performed. Two standard atmospheric simulations were specified as part of the model intercomparison: global transport of short-lived gases, and photodissociation and chemical tendencies in tropospheric air parcels.

A third model intercomparison on simulation of a methane increase in today's atmosphere (also a part of IPCC, 1994) is also included in Section 7.5. This serves as the only example in this chapter of possible future changes in tropospheric ozone due to changes in ozone precursors. The previous ozone assessment (WMO, 1992) includes a thorough discussion of future changes in ozone due to changes in several precursor gases.

7.2 3-D SIMULATIONS OF THE PRESENT-DAY ATMOSPHERE: EVALUATION WITH OBSERVATIONS

7.2.1 Atmospheric Transport

Transport of chemical species in global 3-D models includes terms from both the grid-resolved circulation (winds) and from parameterized subgrid processes (convection, small-scale eddies). A number of recent studies have used chemical tracers with well-known sources and sinks to test specific features of model transport: interhemispheric exchange with chlorofluorocarbons (CFCs) and [85]Kr (Prather *et al.*, 1987; Jacob *et al.*, 1987); convection over continents and long-range transport of continental air to the oceans with [222]Rn (Jacob and Prather, 1990; Feichter and Crutzen, 1990; Balkanski and Jacob, 1990; Balkanski *et al.*, 1992); transport and deposition of aerosols with ^{210}Pb and [7]Be

(Brost *et al.*, 1991; Feichter *et al.*, 1991; Balkanski *et al.*, 1993). These simulations show that global 3-D models can provide a credible representation of atmospheric transport on both global and regional scales. Some major difficulties remain in simulating subgrid processes involved in interhemispheric exchange, convective mass transport, and wet deposition of aerosols. Work is also needed to test the simulation of stratosphere-troposphere exchange; chemical tracers such as bomb-generated $^{14}CO_2$ can be used for that purpose.

7.2.2 Nitrogen Oxides

Global 3-D simulations of NO_x and nitric acid (HNO_3) including sources from combustion, lightning, soils, and stratospheric injection have been reported by Crutzen and Zimmerman (1991) and Penner *et al.* (1991). The Geophysical Fluid Dynamics Laboratory (GFDL) 3-D model with three transported species (NO_x, peroxyacetyl nitrate (PAN), and HNO_3) has been used to simulate the global distributions of NO_y and individual reactive nitrogen species resulting from stratospheric injection (Kasibhatla *et al.*, 1991), fossil fuel combustion (Kasibhatla *et al.*, 1993), and aircraft (Kasibhatla, 1993). The same model including all sources of NO_x has been used to simulate the pre-industrial, present, and future deposition of nitrate (Galloway *et al.*, 1994) and the impact of pollution-generated O_3 on the world's crop production (Chameides *et al.*, 1994). The Oslo 3-D model has been used to study the global distribution of NO_x and NO_y (Berntsen and Isaksen, 1994).

The models of NO_x and NO_y have been, in general, fairly successful at reproducing observations in polluted regions. Concentrations of NO_x in remote regions of the troposphere (*e.g.*, the south Pacific) tend to be underestimated, sometimes by more than an order of magnitude. Possible explanations include an underestimate of the lightning source (Penner *et al.*, 1991), and chemical cycling between NO_x and its oxidation products by mechanisms that are not yet well understood (Chatfield, 1994; Fan *et al.*, 1994).

7.2.3 Hydroxyl Radical

Estimates of the global OH distribution have been made in a number of 3-D model studies of long-lived gases removed from the atmosphere by reaction with OH (Spivakovsky *et al.*, 1990a, b; Crutzen and Zimmerman, 1991; Fung *et al.*, 1991; Tie *et al.*, 1992; Easter *et al.*, 1993; Berntsen and Isaksen, 1994). These estimates have generally been done by using climatological distributions for the principal chemical variables involved in OH production and loss (O_3, NO_x, CO, CH_4) and computing OH concentrations with a photochemical model. Exceptions are the works of Crutzen and Zimmerman (1991) and Berntsen and Isaksen (1994), where O_3 and NO_x concentrations were computed within the model in a manner consistent with the computation of OH concentrations. The accuracy of the global mean OH concentration obtained by the various models appears to be within 30%, as indicated by simulations of methyl chloroform, CH_3CCl_3 (Spivakovsky *et al.*, 1990a; Tie *et al.*, 1992). The seasonality of OH at midlatitudes appears to be well captured, as indicated by a recent simulation of ^{14}CO (Spivakovsky and Balkanski, 1994).

7.2.4 Continental-Scale Simulations of Ozone

The budget of ozone over the North American continent in summer was examined recently using the results of a 3-D model simulation (Jacob *et al.*, 1993a, b). The model was evaluated by comparison with measurements of ozone, NO_x, carbon monoxide (CO), and hydrocarbons. The model captures successfully the development of regional high-ozone episodes over the eastern U.S. on the back side of weak, warm, stagnant anticyclones. Ozone production over the U.S. is strongly NO_x-limited, reflecting the dominance of rural areas as sources of ozone on the regional scale. About 70% of the net ozone production in the U.S. boundary layer is exported, while the rest is deposited within the region. Only 6% of NO_x emitted in the U.S. is exported out of the boundary layer as NO_x or peroxy-acyl nitrates (*e.g.*, PAN), but this export contributes disproportionately to the U.S. influence on global tropospheric ozone because of the high ozone production efficiency per unit NO_x in remote air. Jacob *et al.* (1993b) estimate that export of U.S. pollution supplies 35 Tg ozone to the global troposphere in summer (90 days), half of which is produced downwind of the U.S., following export of NO_x. Recent comparison of O_3-CO correlation in the model and in the observations at sites in the United States and downwind lends support to the model estimate for export of O_3 pollution from North America (Chin *et al.*, 1994).

The ozone model of EMEP MSC-W (European Monitoring and Evaluation Programme, Meteorological

Synthesizing Centre-West) has been used to study photochemistry over Europe for two extended summer periods in 1985 and 1989 (Simpson, 1993), in combination with observations made in the EMEP program. The model describes the boundary layer, combining trajectories in a regular geographical grid over Europe. It is different from the models listed in Table 7-1, and is limited in the context of large-scale ozone modeling mainly by its neglect of explicit representation of free tropospheric processes. Significant differences in the concentrations of the photo-oxidants were observed and modeled between the two summer seasons that were studied. The modeled ozone concentrations compare satisfactorily with observations, particularly in 1989. The study showed that NO_x limits ozone formation in the European boundary layer in most locations, whereas NMHCs limit the production mostly in polluted areas.

Flatøy et al. (1994) present results from a set of simulations with a three-dimensional mesoscale chemistry transport model driven by meteorological data from a numerical weather prediction model with an extensive treatment of cloud physics and precipitation processes. New formulations for the vertical transport of chemical tracers in connection with convective plumes and the compensating sinking motion, and the calculation of photolysis rates in clouds, are employed. The chemistry transport model is used to calculate ozone and other chemical species over Europe over a 10-day period in July 1991, characterized by warm weather and frequent cumulus episodes. When modeled vertical ozone profiles are compared to ozone soundings, better correlation is found than for calculation without convection, indicating that physical processes, especially convection, can dominate in the vertical distribution of ozone in the free troposphere, and that sinking air that compensates for convective updrafts is important for the tropospheric ozone budget.

7.3 CURRENT TROPOSPHERIC OZONE MODELING

Modeling tropospheric ozone is probably one of the most difficult tasks in atmospheric chemistry. This is due not only to the large number of processes that control tropospheric ozone, but even more to interactions of processes occurring on different spatial and temporal

scales (Section 7.1, Figure 7-1). The field of tropospheric ozone modeling is currently under rapid development.

To cover various spatial scales with limited computer resources, different types of models have been used. 2-D models have been widely used for several years to study tropospheric ozone on a global scale. 3-D models covering the global scale have only recently been developed. An accurate representation of the 3-D transport is needed in models, especially in order to describe distributions of species with a chemical lifetime of the order of days or weeks (like NO_x and ozone) in areas where the transport is efficient, as, e.g., in convective cells.

7.3.1 Global and Continental-Scale Models

CATEGORIES OF MODELS

Several chemistry transport models (CTMs) have been used to study ozone and precursor molecules in the troposphere and in general to understand processes and budgets of atmospheric constituents. A list of models is given in Table 7-1, where models have been grouped in four categories.

The first group is 2-D zonally averaged models. Such models have been used for several years to study global distributions of ozone and precursors in the current atmosphere. To represent the various processes explained in Figure 7-1, they contain detailed and relatively similar schemes of ozone photochemistry. The transport is described by a meridional circulation, and relatively large diffusion is included to account for transport due to wave activity. Only a few 2-D models represent convection explicitly. Most of the models have been used to study changes in ozone, some in the past and most of the models in the future, due to changes in emissions of ozone precursors (NO_x, CH_4, CO, NMHC; see Figure 7-1) and in physical variables such as temperature, water vapor, and UV radiation. With currently available computing resources, such models can, e.g., be used to predict ozone changes over several decades for a range of trace gas emission scenarios.

The next three categories contain 3-D models. One group of 3-D models uses monthly averaged wind fields to transport tracers, and therefore also need relatively efficient diffusion to account for transport due to winds that change on a day-to-day basis. However, the

Table 7-1. Current 2-D (global) and 3-D (global and mesoscale) Chemistry-Transport Models.

Model	References
2-D models	
UK Met Office	Derwent (1994)
Harwell	Johnson (1993); Johnson *et al.* (1992)
Univ Cambridge	Law and Pyle (1993a, b)
Univ Oslo	Fuglestvedt *et al.* (1994a, b)
Univ Bergen	Strand and Hov (1993; 1994)
TNO	Roemer and van der Hout (1992)
NCAR/CNRS	Hauglustaine *et al.* (1994)
MPI-tropo	Singh and Kanakidou (1993); Kanakidou *et al.* (1991)
LLNL	Wuebbles *et al.* (1993); Patten *et al.* (1994)
3-D monthly average	
Moguntia	Lelieveld (1994)
Images	Müller and Brasseur (1994)
3-D synoptic global	
LLNL	Penner *et al.* (1991; 1994)
GFDL/GIT	Kasibhatla *et al.* (1991; 1993)
GISS/Harvard	Spivakovsky *et al.* (1990a, b)
Univ Oslo	Berntsen and Isaksen (1994)
3-D synoptic mesoscale	
GISS/Harvard	Jacob *et al.* (1993a, b)
Univ Bergen	Flatøy (1994); Flatøy *et al.* (1994)

TNO = Netherlands Organization for Applied Scientific Research; NCAR = National Center for Atmospheric Research; CNRS = Centre National de la Recherche Scientifique; MPI = Max-Planck Institute; LLNL = Lawrence Livermore National Laboratory; GFDL = Geophysical Fluid Dynamics Laboratory; GIT = Georgia Institute of Technology; GISS = Goddard Institute for Space Studies

models in this category include detailed photochemical schemes. In the last two categories, the models use daily varying windfields and describe either the global scale or mesoscales. Only recently, 3-D models of this category have been developed to include detailed ozone chemistry. Applications and further development of such models are expected in the near future. Some models included in Table 7-1 have been used to study other trace gases, *e.g.*, NO_y. Work is currently going on to include ozone chemistry in some of these models.

MODELED OZONE DISTRIBUTIONS

Zonally averaged ozone distributions from several of the models listed in Table 7-1 are shown in Figure 7-2. The distributions that are shown are all for near-solstice conditions, for January and July. Although all model results represent the current atmosphere, there are differences between the models in the choices of boundary conditions and in the emissions of chemical ozone precursors.

The models agree on the general feature of the zonally averaged ozone distribution. The vertical distri-
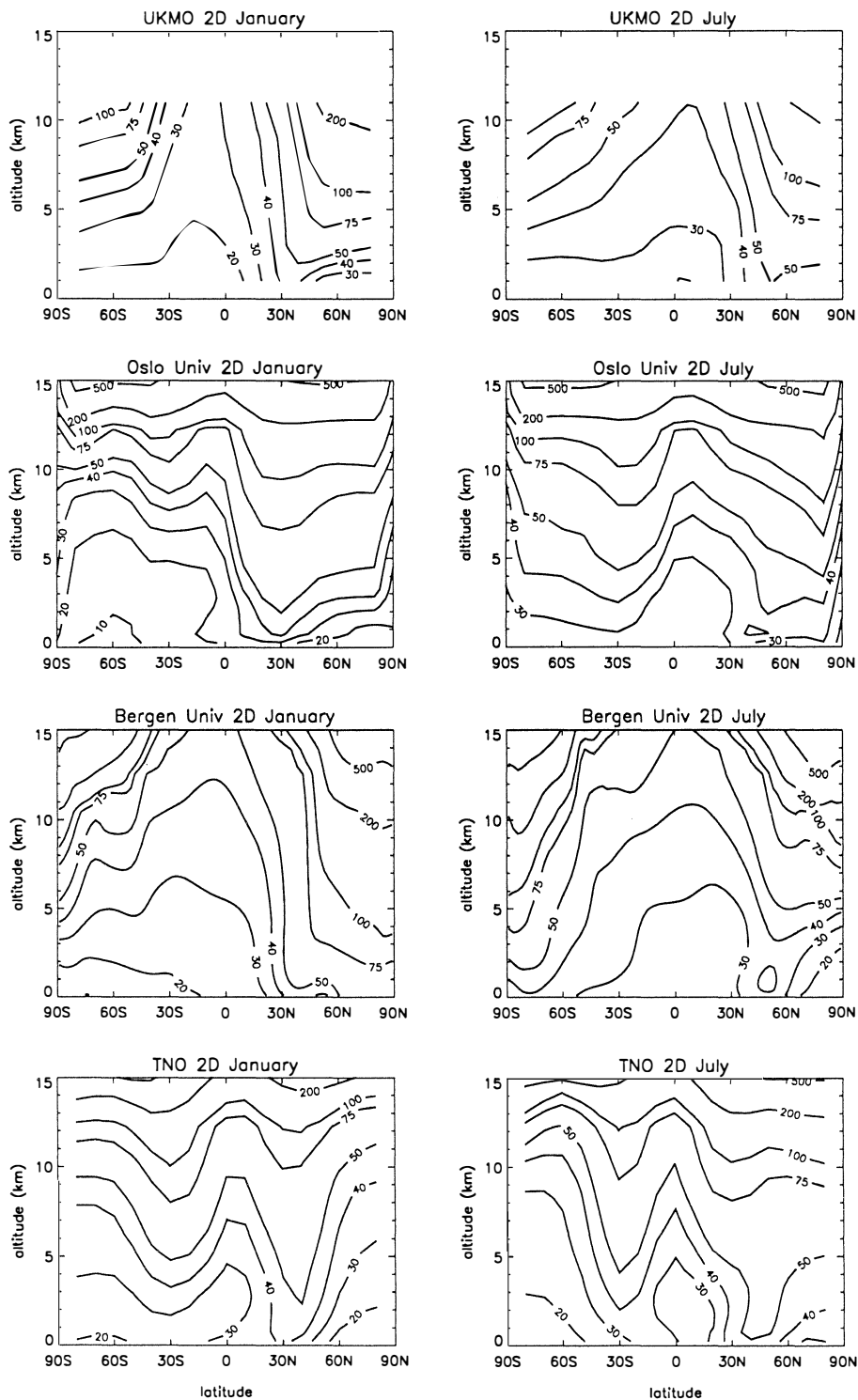
Figure 7-2. Latitude by altitude contours of zonally averaged ozone mixing ratios as calculated in eight global ozone models. The models are listed in Table 7-1. Data represent mid-January and mid-July conditions for the current atmosphere. (Continued on page 7.9.)

Figure 7-2, continued.
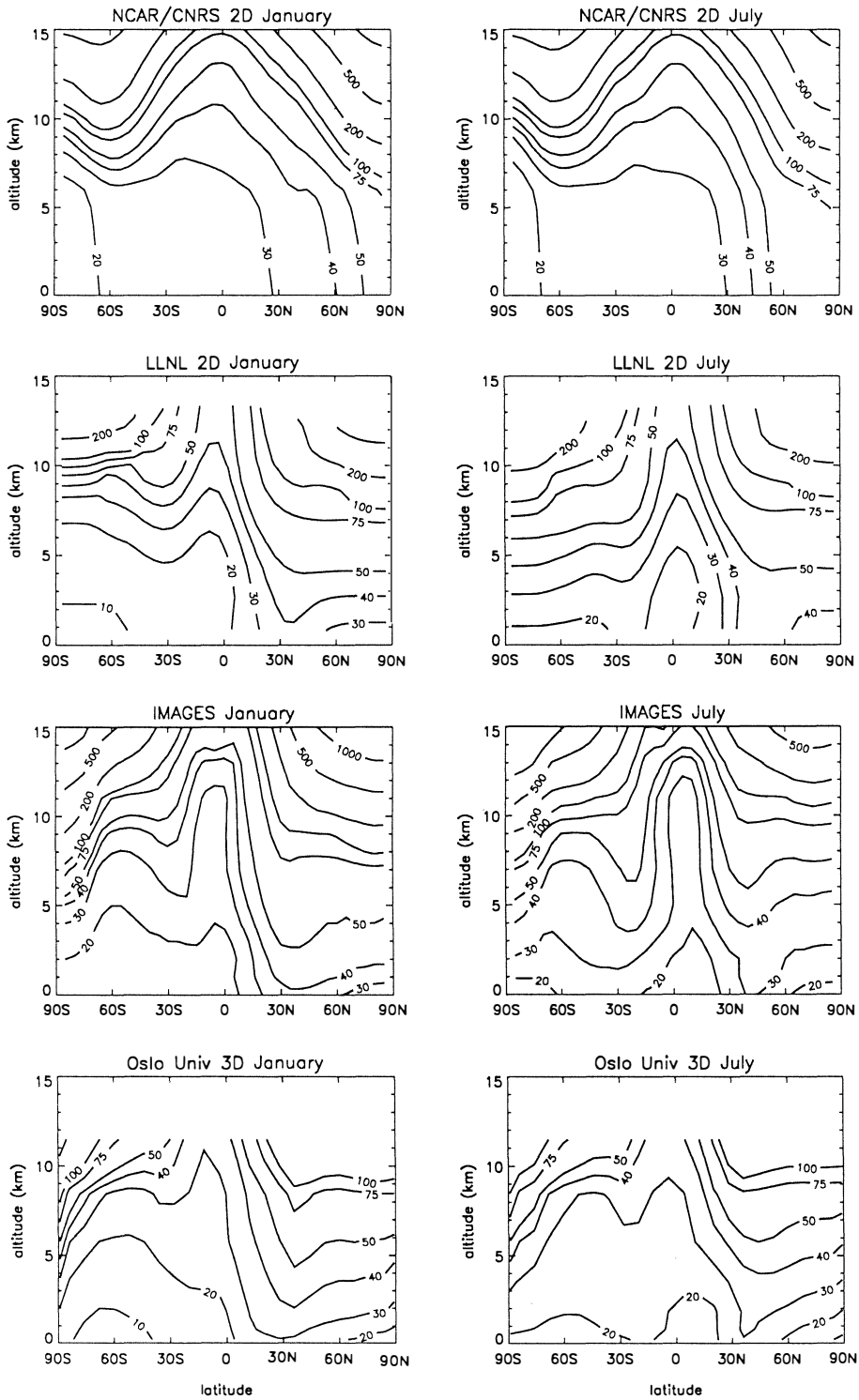
bution, with maximum values in the upper troposphere and minimum values at the surface, reflects mainly the import of ozone from the stratosphere and deposition at the ground. It is also clear that current global tropospheric ozone models are able to reproduce gross features of observed ozone distributions (see Section 7.5.3 below).

The modeled mixing ratios in the tropics at the 10 km level are in the range 40-60 ppb and the boundary layer values about 10-30 ppb. Generally the models give higher ozone mixing ratios over the Northern Hemisphere (NH) than over the Southern Hemisphere (SH) during summertime. The modeled ozone levels in the lowest few kilometers at northern middle latitudes are in the range 30-50 ppb in July. In January the corresponding values are 10-30 ppb in the SH. Comparison and interpretation of the ozone levels in the region of largest importance for radiative forcing (upper troposphere/ lower stratosphere) are difficult due to insufficient information about the tropopause levels in the models. The ozone levels in this region are to a high degree determined by processes in the lower stratosphere, where ozone mixing ratios or fluxes through the tropopause are fixed in most models. The latitudinal distribution varies considerably between the models, reflecting clearly the efficiency of the horizontal diffusion adopted in the model, as discussed below in Section 7.5.2, with the least latitudinal gradients in some of the 2-D models.

GLOBAL OZONE BUDGETS

From some of the models listed in Table 7-1, global budget numbers are available that can be used to explore the relative roles of the processes governing tropospheric ozone, as explained in Figure 7-1. Stratosphere/troposphere exchange, photochemical reactions, and surface deposition are identified as the three major classes of processes governing the tropospheric ozone budget. There are substantial differences between the relative importance of these processes, in the way they are represented in current models, as can be seen from Table 7-2.

There is a factor 3 spread in the stratosphere/troposphere exchange fluxes and the surface deposition values between the models. This merely reflects the large uncertainty in our knowledge of the efficiency of these processes. The models usually either fix the flux through the tropopause or fix the ozone mixing ratios in the lower stratosphere, strongly tying the flux to observations. The most recent estimate of the ozone flux across the tropopause is based on aircraft measurements (Murphy *et al.*, 1993; see discussion in Chapter 5), yielding values in the range 240-820 Tg (O_3)/yr, which are comparable with or slightly less than previous estimates (Danielsen and Mohnen, 1977; Gidel and Shapiro, 1980; Mahlman *et al.*, 1980; see also Chapter 5). The spread in values for surface deposition is presumably reflecting differences in, *e.g.*, vertical transport through the boundary layer. Observations that can narrow the uncertainty in its efficiency do not exist. There is currently therefore little basis for judging which models calculate the most realistic tropospheric ozone budget terms.

The even larger differences in the budgets for net photochemical production of ozone (more than a factor 6) do not necessarily imply that the photochemical schemes in the models are very different. The net production is a small difference between large production and sink terms. This is illustrated in Table 7-2, showing also globally integrated values for the most important individual source and loss mechanisms (see Chapter 5) in one 2-D model (Derwent, 1994). In this model the total production and the total loss is about 4 times larger than the flux from the stratosphere, whereas the net production comes out as a number that is much smaller than the stratospheric flux.

It is obvious that differences in the import and export terms also influence the net chemical production, since the budget balances in the models. A model that, *e.g.*, has a large import from the stratosphere or an inefficient deposition at the ground, estimates high ozone concentrations in the troposphere, thereby increasing the chemical loss, since the ozone (or excited atomic oxygen produced from ozone) participates itself in the loss reactions (see Chapter 5 and Table 7-2), and since the photolysis of ozone initiates oxidation processes influencing production as well as loss reactions for ozone.

ASPECTS OF ZONAL ASYMMETRIES

Two-dimensional tropospheric chemistry models calculate zonally averaged trace gas distributions, and therefore neglect zonal asymmetries. Yet they capture the coarse features of the ozone distribution and they are useful tools for sensitivity studies and analyses. Howev-

Table 7-2. Examples of globally integrated budget terms for tropospheric ozone, for the current and pre-industrial atmospheres, as calculated in various models, in Tg (O_3)/yr.

Model/Investigator	Ref.	Present atmosphere			Pre-industrial atmosphere		
		Chem[a]	Strat[b]	Dep[c]	Chem	Strat	Dep
UOslo 3-D/Berntsen	(1)	295	846	-1178			
Moguntia 3-D/Lelieveld	(2)	427	528	-953	-87	552	-465
Cambridge 2-D/Law	(3)	1021	601	-1622			
UKMO 2-D/Derwent	(4)	343*	1077	-1420			
TNO 2-D/Roemer	(5)	728	962	-1690	-195	962	-767
CNRS/NCAR 2-D/ Hauglustaine	(6)	216	408	-612	-75	458	-424
UBergen 2-D/Strand	(7)	1404	533	-1937			
AER 2-D/Kotomarthi	(8)	416	610	-1026			

a) Chem: The numbers represent net photochemical production, which is a small difference between large production and loss terms (see text and the panel below). Since the budgets balance, net chemical production must respond to stratosphere/troposphere exchange and surface deposition by changing the ozone abundances.

b) Strat: Net flux from the stratosphere to the troposphere, fixed or parameterized in the models.

c) Dep: Surface deposition.

(1) Berntsen and Isaksen (1994)
(2) Lelieveld (1994)
(3) Law and Pyle (1993a, b) + personal communication
(4) Derwent (1994) + personal communication
(5) Roemer and van der Hout (1992)
(6) Hauglustaine *et al.* (1994)
(7) Strand and Hov (1994)
(8) Kotomarthi, personal communication. AER = Atmospheric and Environmental Research, Inc.

* Individual chemical terms are as follows:

Term	Strength	
$HO_2 + NO$	3117	
$CH_3O_2 + NO$	1006	
$RO_2 + NO$	462	
Total production		4585
$O(^1D) + H_2O$	-1704	
$O_3 + OH$	-410	
$O_3 + HO_2$	-1719	
$O_3 + NMHC$	-178	
$O_3 + NO$ (net loss)	-177	
$O(^3P)$ (net loss)	-54	
Total loss		-4242
Net chemical production		343

er, quantitative assessments based on these models will remain uncertain, due to limitations in their ability to simulate realistically global transport of tracers (see Section 7.5.2), and due to the lack of possibility to resolve longitudinal variations in several species of key importance for the ozone chemistry, in particular in NO_x mixing ratios, observed between continental and oceanic regions. The errors resulting from the assumption of longitudinally uniform emissions have been evaluated by use of a 3-D global monthly averaged model (Kanakidou and Crutzen, 1993). Longitudinally varying NO, C_2H_6, and C_3H_8 emissions lead to significantly lower O_3 and OH concentrations, especially in the middle and low troposphere in the tropics and at northern midlatitudes, than when zonally averaged emissions were used. The computed discord varies with latitude and height and was locally as high as 80% for OH concentrations in the tropics and 60% at midlatitudes.

On the other hand, there is no guarantee that 3-dimensional models can simulate correctly the NO_x distributions and total nitrate observations in the troposphere and, in particular, in remote marine locations (Penner et al., 1991; Kasibhatla et al., 1993; Gallardo et al., 1994). This can be due to limitations in knowledge of emissions, but also in the simulation of atmospheric chemistry and transport from source areas in the model. For example, Gallardo et al. (1994), testing various scenarios of distribution of NO_x emissions from lightning, found that a convection-related lightning distribution could improve considerably the agreement with observations of NO_x and total nitrate in remote oceanic areas.

THE ROLE OF CONVECTION

Representation of convection in global models requires parameterization, due to the small scale of the process. It therefore needs special consideration. One consequence of convection is that ozone precursors (NO_x, CO, and NMHC), once they are transported to the free troposphere, have a longer chemical lifetime, allowing them to be transported over long distances and contribute to ozone formation downwind of the convective cell. This has been confirmed in a model study of deep tropical convection events observed during the Amazon Boundary Layer Experiment 2A (ABLE 2A), showing enhanced ozone formation in the middle and upper troposphere (Pickering et al., 1992). Meteorolog-

ical and trace gas observations from convective episodes were analyzed in the study with models of cumulus convection and photochemistry. The level of formation of free tropospheric ozone was shown to depend on the surface trace gas emissions entrained in the cumulus convective events.

On the other hand, boundary layer air poor in NO_x depresses the upper tropospheric ozone formation following convective events. This was found in a study based on aircraft data from the Stratosphere-Troposphere Exchange Project (STEP) and the Equatorial Mesoscale Experiment (EMEX) flights off northern Australia, again using cumulus cloud and photochemical models (Pickering et al., 1993). A 15-20% reduction in the rate of O_3 production between 15 and 17 km was the largest perturbation calculated for these experiments due to convection events. The study also showed that O_3 production between 12 and 17 km would slow down by a factor of 2 to 3 in the absence of NO_x from lightning.

A secondary effect of deep cumulus convection is associated with downward transport of ozone and NO_x-rich air from the upper troposphere in the cumulus downdrafts. The downward transport of ozone and NO_x brings these components into regions where their lifetime is much shorter than in the upper troposphere. Lelieveld and Crutzen (1994) have used a 3-D global model to quantify this effect. Their calculations give a decrease in total tropospheric ozone concentrations of 20% when deep convection is included in the calculations. The results are partly due to a corresponding decrease in the global column of NO_x of about 30%. However, the decreased downward transport of ozone resulted in an increase in the oxidation capacity of the troposphere. Inclusion of convection increased methane destruction by about 20% and CO destruction by about 10%.

7.3.2 Limitations in Global Models

Modeling of ozone production in the troposphere is very sensitive to the assumed strengths and distribution of sources of ozone precursors. Estimates of emissions, in particular of natural NO_x (lightning and surface sources) and hydrocarbons (isoprene and terpenes), are associated with large uncertainties that yield uncertainties also in modeled ozone production. Accurate emission data of O_3 precursors are clearly needed to correctly simulate tropospheric chemistry.

A global CTM needs to represent the transport of trace gases from their source to their sink regions. The mass flux can be formulated as a function of the wind velocity. The spatial and temporal resolution of wind data, as provided by data assimilation or models, is limited. Advection in a CTM therefore captures only a fraction of the total transport, and sub-grid processes need to be parameterized, limiting the accuracy of transport of ozone and other trace gases in the CTM. Such sub-grid processes include transport within the boundary layer, exchange between the boundary layer and the free troposphere, convective transport, small-scale mixing processes, and tropopause exchange. Inaccuracies in model representation of sub-grid processes is of largest importance for trace gases with lifetimes of the order of days or weeks, like ozone and NO_x. This is of particular importance since NO_x influences ozone chemically in a nonlinear way.

A variety of heterogeneous chemical reactions can affect the tropospheric ozone budget. The accuracy of global ozone models is limited by the fact that the paths and rates of such reactions are uncertain and by the fact that such processes take place on spatial scales that are not resolved in global models. Such heterogeneous reactions include oxidation of N_2O_5 to nitrate, loss reactions for ozone, removal of formaldehyde, and the separation of chemical ozone precursors inside (HO_2) and outside (NO) cloud water droplets.

Gas phase chemical kinetics and photochemical parameters are reasonably well established. However, calculation of photodissociation rates is difficult in regions with clouds and aerosols, due to difficulties in model representation of optical properties, and the small spatial and temporal scale of clouds.

A wide range of hydrocarbons take part in ozone production in the troposphere in the presence of NO_x. The formulations of the degradation mechanisms of hydrocarbons can be important sources of uncertainty in tropospheric ozone models. The oxidation chains of the dominant natural hydrocarbons, isoprene and terpenes, are still not well known. Furthermore, the number of emitted hydrocarbons is so large that they can only be represented in models in groups (lumped species).

Finally, development of global ozone models is hampered by the lack of extensive data sets for observed species distributions. In order to test and validate models, measurements are needed for several key species on synoptic and even smaller scales.

7.4 APPLICATIONS

Numerical models offer the possibility to assess the role of certain processes on a global scale. This section presents some selected applications of models, when they have been used to perform global integration of key processes of importance for tropospheric chemistry and the ozone budget.

7.4.1 Global Tropospheric OH

The hydroxyl radical, OH, is produced from O_3 following photolysis to the excited state $O(^1D)$ and its reaction with H_2O. In turn, the HO_x family (OH, HO_2, H_2O_2) is involved in the production of tropospheric O_3 in reactions with NO_x (NO + NO_2). The reaction of OH with NO_2 also provides the terminating step in NO_x-catalyzed production of O_3 by converting NO_x into HNO_3. Furthermore, HO_x also removes ozone in NO_x-poor environments. Thus the tropospheric chemistry of O_3 and OH are intertwined, and any possible calibration of modeled OH adds confidence to the simulation of tropospheric O_3.

OH concentrations respond almost instantly to variations in sunlight, H_2O, O_3, NO and NO_2 (NO_x), CO, CH_4, and NMHC; and therefore the OH field varies by orders of magnitude in space and time. Observations of OH can be used to test the photochemical models under specific circumstances, but are not capable of measuring the global OH field. Therefore we must rely on numerical models and surrogates to provide the global and seasonal distribution of OH; these models need to simulate the variations in sunlight caused by clouds and time-of-day in addition to the chemical fields. These calculations of global tropospheric OH and the consequent derivations of lifetimes have not changed significantly and are still much the same as in the AFEAS (Alternative Fluorocarbons Environmental Acceptability Study) Report (WMO, 1990); we cannot expect such calculations to achieve an accuracy much better than ±30%.

We can derive some properties of the global OH distribution by observations of trace gases whose abundance is controlled by reactions with OH, in conjunction

with some model for their emissions and atmospheric mixing. For example, the trace gases methyl chloroform (CH_3CCl_3), [14]CO, and HCFC-22 have been used to derive empirical OH and thus test the modeled OH fields. These gases (1) are moderately well mixed, (2) have well calibrated and well measured atmospheric burdens, and (3) have small or well defined other losses. However, they primarily test only the globally, annually averaged OH concentration, and even this average quantity is weighted by the distribution and reaction rate coefficient of OH with the gas. Some model studies have used CH_3CCl_3 (Spivakovsky *et al.*, 1990a) and [14]CO (Derwent, 1994) to test their ab initio calculations of tropospheric OH. Such studies have argued that the observed seasonal distributions support the modeled seasonal distribution of OH, but such seasonality also results from transport and depends on the rate of mixing between the aseasonal tropics and the midlatitudes.

The lifetimes for many ozone-depleting and greenhouse gases depend on tropospheric OH, and at this stage of model development we rely on the empirical values. CH_3CCl_3 fulfills all of the above requirements for calibrating tropospheric OH. It has the further advantage that its tropospheric distribution and reaction rate are similar to many of the other gases in which we are interested. A recent assessment (Kaye *et al.*, 1994) has reviewed and re-evaluated the lifetimes of two major industrial halocarbons, methyl chloroform (CH_3CCl_3) and CFC-11. An optimal fit to the observed concentrations of CH_3CCl_3 from the five Atmospheric Lifetime Experiment/Global Atmospheric Gases Experiment (ALE/GAGE) surface sites over the period 1978-1990 was done with a pair of statistical/atmospheric models (see Chapter 3 in Kaye *et al.*, 1994). The largest uncertainty in the empirical CH_3CCl_3 lifetime, 5.4 ± 0.6 yr, lies currently with the absolute calibration. The implication of a trend in this lifetime, presumably due to a change in tropospheric OH (Prinn *et al.*, 1992), is sensitive to the choice of absolute calibration. Analyses of the tropospheric budgets of the radio-isotope [14]CO (Derwent, 1994) and HCFC-22 (Montzka *et al.*, 1993) complement this analysis and confirm the empirical estimate of tropospheric OH.

7.4.2 Budgets of NO_y

Concentrations of NO_x are critical for ozone production. A central difficulty in modeling global ozone is to predict the distribution of NO_y components including the large variability observed on small scales, the transport out of the boundary layer, and chemical recycling of nitrogen reservoir species. It is a problem that the relative roles of sources of tropospheric NO_x (surface emissions, lightning, transport from the stratosphere, and aircraft emissions) in generating observed levels are not quantitatively well known. This section describes a few recent model studies addressing the role of emissions, transport, and chemical conversion of reactive nitrogen compounds.

A 3-D global chemistry-transport model has been used to assess the impact of fossil fuel combustion emissions on the fate and distribution of NO_y components in various regions of the troposphere (Kasibhatla *et al.*, 1993). It was found that wet and dry deposition of NO_y in source regions remove 30% and 40-45% of the emissions, respectively, with the remainder being exported over the adjacent ocean basins. The fossil fuel source was found to account for a large fraction of the observed surface concentrations and wet deposition fluxes of HNO_3 in the extratropical North Atlantic, but to have a minor impact on NO_y levels in the remote tropics and in the Southern Hemisphere.

Another global 3-D model study has calculated the effect of organic nitrates, which can act as reservoirs for NO_x and therefore redistribute NO_x in the troposphere (Kanakidou *et al.*, 1992). During their chemical formation, the organic nitrates may capture NO_x that can be released after transport and subsequent decomposition away from source regions. The importance of hydrocarbons in the formation of peroxyacetyl nitrate (PAN), which is the most abundant nitrate measured in the troposphere, was demonstrated in the study, which also included comparison with observations. According to the model calculations, the efficiency of acetone in producing PAN in the middle and high troposphere of the NH ranges between 20 and 25%. This relationship between acetone and PAN concentrations has also been observed during the Arctic Boundary Layer Expedition (ABLE) 3B experiment. The observed concentrations of acetone and PAN were much higher than those calculated by the model, which takes into account ethane and propane photochemistry only. Consideration of the oxidation of higher hydrocarbons and of direct emissions of acetone is therefore needed to explain the observed concentrations (Singh *et al.*, 1994).

An analysis of data from ABLE-3A using a photochemical model has shown that PAN and other organic nitrates act as reservoir species at high latitudes for NO_x that is mainly of anthropogenic origin, with a minor component from NO_x of stratospheric origin (Jacob et al., 1992). This tropospheric reservoir of nitrogen is counteracting O_3 photochemical loss over western Alaska relative to a NO_x-free environment. The concentrations of O_3 in the Arctic and sub-arctic troposphere have been found to be regulated mainly by input from the stratosphere and losses of comparable magnitude from photochemistry and deposition (Singh, et al., 1992; Jacob et al., 1992).

Based on 2-D model calculations, the previous ozone assessment (WMO, 1992) showed that injection of NO_x directly into the upper troposphere from commercial aircraft is substantially more efficient in producing ozone than surface-emitted NO_x. Model tests that have been performed show that the ozone-forming potential of NO_x emitted from airplanes depends on, e.g., transport formulation, injection height, and the removal rate. Furthermore, making reliable quantitative estimates of the ozone production due to the aircraft emission is also difficult, as it is nonlinear and it depends strongly on the natural emissions and the background concentrations of NO_x, which are not well characterized (see discussion in Chapter 11).

7.4.3 Changes in Tropospheric UV

Reductions in ozone column densities due to enhanced ozone loss in the stratosphere will lead to enhanced UV penetration to the troposphere, causing chemical changes. Such increased UV levels have been observed in connection with reduced ozone column densities during the last few years (WMO, 1992; Smith et al., 1993; Kerr and McElroy, 1993; Gleason et al., 1993). The significance for tropospheric chemistry of enhanced UV fluxes is that they affect the lifetimes of key atmospheric compounds like CO, CH_4, NMHC, hydrofluorocarbons (HFCs), and hydrochlorofluorocarbons (HCFCs) and the photochemical production and loss of tropospheric ozone (Liu and Trainer, 1988; Brühl and Crutzen, 1989; Madronich and Granier, 1992; Fuglestvedt et al., 1994a). The main cause of this change is that enhanced UV radiation increases $O(^1D)$ production, which in turn will lead to enhanced tropospheric OH levels.

The atmospheric lifetimes of the above-mentioned chemical compounds will be reduced since reactions with OH represent the main sink. The reduced growth rate of CH_4 that has been observed during the last decade could, at least partly, be due to decreased lifetime resulting from enhanced UV fluxes. Fuglestvedt et al. (1994a) have estimated that approximately 1/3 of the observed reduction in growth rate during the 1980s is due to enhanced UV radiation resulting from reduced ozone column densities over the same time period. In the same study it was found that tropospheric ozone was reduced in most regions. It was only at middle and high northern latitudes during limited time periods in the spring where NO_x levels were sufficiently high, that ozone was increased due to enhanced UV radiation. There might also be significant changes in UV radiation, and thereby in chemical activity, due to changes in the reflecting cloud cover and due to backscatter by anthropogenic sulfate aerosols (Liu et al., 1991). Marked changes in the ratio of scattered UV-B radiation to direct radiation have also been observed in New Zealand after the Mount Pinatubo eruption (see Chapter 9).

7.4.4 Changes Since Pre-industrial Times

Measurements of the chemical composition of air samples extracted from ice cores have been compared to measurements of the present atmosphere, revealing that methane volume mixing ratios have increased from about 800 ppb to about 1700 ppb since the pre-industrial period (see Chapter 2). The methane increase may have reduced the OH concentration and the oxidizing efficiency of the atmosphere. However, an increase in production of ozone and thus also OH will also accompany growing CH_4 levels. As a result of industrialization, extensive anthropogenic emissions of the ozone precursors CO, NO_x, and NMHC have also occurred, increasing ozone on a local and regional scale and, to a lesser extent, on a global scale.

The temporal trends in tropospheric ozone in the past are difficult to calculate particularly because of the critical role of surface NO_x emissions. A few model studies of impacts of anthropogenic emissions since pre-industrial times predict large increases in ozone (Roemer and van der Hout, 1992; Hauglustaine et al., 1994; Lelieveld, 1994). The predicted changes in ozone during the time of industrialization are not inconsistent with observations (see Chapter 1). Predictions of ozone change

have, however, only been made with a limited number of models. It has been done with models describing in principle the main processes governing the ozone budget. However, more detailed models are needed to calculate quantitatively reliable temporal trends in ozone.

A few models have estimated globally averaged strengths of the various budget terms for ozone under pre-industrial conditions. The numbers are given in Table 7-2. Only changes in emissions of gases like CH_4, CO, NO_x, and NMHC have been considered in the model experiments, whereas the meteorology and the transport of atmospheric species have been assumed to be unchanged. Despite the wide spread in the strength of individual processes regulating global tropospheric ozone (Section 7.3.1), there is good agreement between the models in the changes in the ozone chemistry that may have occurred during the time of industrialization. According to the model calculations, both production and loss were weaker in pre-industrial times, and the chemistry has changed from being a net sink to a net source of ozone. The global burden of tropospheric ozone increased in these model studies by 55-70% over the time of industrialization, supporting the assumption that the observed marked increase in ozone over the last approximately 100 years has at least partly been due to anthropogenic emissions.

In a review paper on the oxidizing capacity of the atmosphere, Thompson (1992) compiled changes in global OH since pre-industrial times as calculated in several global models. There is consensus that OH has decreased globally since the pre-industrial times. However, there is a substantial spread in the estimates, which range from only a few to about 20%.

7.5 INTERCOMPARISON OF TROPOSPHERIC CHEMISTRY/TRANSPORT MODELS

The observed changes in the cycles of many atmospheric trace gases are expected, and often observed, to produce a chemical response. For example, we have accumulated evidence that tropospheric ozone in the northern midlatitudes has increased substantially, on the order of 25 ppb, since pre-industrial times. During this period, the global atmospheric concentration of CH_4 has increased regularly, and the emissions of NO_x and NMHC, at least over northern midlatitudes, have also increased greatly. An accounting of the cause of the O_3

increases, particularly to any specific emissions, requires a global tropospheric CTM, preferably a 3-D model. A CTM provides the framework for coupling different chemical perturbations that are, by definition, indirect and thus cannot be evaluated simply with linear, empirical analyses. We are placing an increasing responsibility on CTM simulations of the atmosphere (*e.g.*, the GWP calculation for CH_4 in IPCC 1994) and should therefore ask how much confidence we have in these models. Models of tropospheric chemistry and transport have not been adequately tested in comparison with those stratospheric models used to assess ozone depletion associated with CFCs (*e.g.*, WMO, 1990, 1992; Prather and Remsberg, 1992). In addition, the greater heterogeneity within the troposphere (*e.g.*, clouds, convection, continental versus marine boundary layer) makes modeling and diagnosing the important chemical processes more difficult. This section presents a beginning, objective evaluation of the global CTMs that simulate tropospheric ozone.

There are numerous published examples of individual model predictions of the changes in tropospheric O_3 and OH in response to a perturbation (*e.g.*, pre-industrial to present, doubling CH_4, aircraft or surface combustion NO_x, stratospheric O_3 depletion). Since these calculations in general used different assumptions about the perturbants or the background atmosphere, it is difficult to use these results to derive an assessment. Further, we need to evaluate how representative those models are with a more controlled set of simulations and diagnostics.

Thus, two model intercomparisons and one assessment are included as part of this report: (1) prescribed tropospheric photochemical calculations that test the modeling of O_3 production and loss; (2) transport of short-lived radon-222 that highlights differences in transport description between 2-D and 3-D global chemical tracer models in the troposphere; and (3) assessing the impact of a 20% increase in CH_4 on tropospheric O_3 and OH. All of these studies were initiated as blind intercomparisons, with model groups submitting results before seeing those of others. The call for participation in (1) and (3) and preliminary specifications went out in June 1993; the first collation of results was reported to the participants in January 1994; and the final deadline for submissions to this report was June 1994. In the transport study, no obvious mistakes in performing the

Table 7-3. Initial values used in PhotoComp.

ALTITUDE	MARINE	LAND+BIO	FREE	PLUME/X + PLUME/HC
(km)	0	0	8	4
T (K)	288.15	288.15	236.21	262.17
p (mbar)	1013.25	1013.25	356.50	616.60
N (#/cm^3)	2.55E19	2.55E19	1.09E19	1.70E19
H$_2$O (% v/v)	1.0	1.0	0.05	0.25
O$_3$ (ppb)	30	30	100	50
NO$_x$ (ppt)	10	200	100	10000
HNO$_3$ (ppt)	100	100	100	100
CO (ppb)	100	100	100	600
CH$_4$ (ppb)	1700	1700	1700	1700
NMHC	none	none	none	see footnote

H$_2$ = 0.5 ppm; H$_2$O$_2$ = 2 ppb for all cases. BIO case equals LAND but with 1 ppb isoprene.
PLUME without NMHCs (/X) and with NMHCs (/HC). Initial values of NMHC (ppb): C$_2$H$_6$ = 25, C$_2$H$_4$ = 40, C$_2$H$_2$ = 15, C$_3$H$_8$ = 15, C$_3$H$_6$ = 12.5, C$_4$H$_{10}$ = 5, toluene = 2, isoprene = 0.5.
(Note: Integrations were performed for 5 days starting July 1, with solar zenith angle 22 degrees.)

case studies were found, and detailed results will be published as a WCRP (World Climate Research Programme) workshop report. In the photochemical study and methane assessment, about half of the results contained some obvious errors in the setup, diagnosis, or model formulation that were found in January 1994. Most participants identified these errors and chose to resubmit new results. Removal or correction of obvious errors did not eliminate discrepancies among the models, and significant differences still remain and are presented here. The current list of contributions is identical to the parallel IPCC Assessment. The combination of these intercomparisons provides an objective, first look at the consistency across current global tropospheric chemical models.

7.5.1 PhotoComp: Intercomparison of Tropospheric Photochemistry

An evaluation of the chemistry in the global CTMs is not easy. There are no clear observational tests of the rapid photochemistry of the troposphere that include the net chemical tendency of O$_3$ and are independent of transport. Furthermore, uncertainties in the kinetic parameters would probably encompass a wide range of observations. Thus, we chose an engineering test (PhotoComp) in which all chemical mechanisms and data, along with initial conditions, were specified exactly as in Table 7-3. Atmospheric conditions were prescribed (July 1, U.S. standard atmosphere with only molecular scattering and O$_2$ + O$_3$ absorption) and the air parcels with specified initial conditions were allowed to evolve in isolation for five days with diurnally varying photolysis rates (J's). PhotoComp becomes, then, a test of the photochemical solvers used by the different groups in which there is only one correct answer. For most of these results, many models give similar answers, resulting in a "band" of consensus, which we assume here to be the correct numerical solution. The 23 different model results submitted to PhotoComp are listed in Table 7-4.

The PhotoComp cases were selected as examples of different chemical environments in the troposphere. The wet boundary layer is the most extensive, chemically active region of the troposphere. Representative conditions for the low-NO$_x$ oceans (case: MARINE) and the high-NO$_x$ continents (case: LAND) were picked. In MARINE, ozone is lost rapidly (-1.4 ppb/ day), but in

Table 7-4. Models participating in the PhotoComp and delta-CH$_4$ intercomparisons.

Code	Affiliation	Contributor*	(e-mail)
A	U. Mich.	Sandy Sillman	(sillman@madlab.sprl.umich.edu)
B	UKMetO/UEAnglia	Dick Derwent	(rgderwent@email.meto.govt.uk)
B&	UEA-Harwell/2-D	Claire Reeves	(c.reeves@uea.ac.uk)
C	U. Iowa	Gregory Carmichael	(gcarmich@icaen.uiowa.edu)
D	UC Irvine	Michael Prather	(prather@halo.ps.uci.edu)
E	NASA Langley	Jennifer Richardson	(richard@sparkle.larc.nasa.gov)
F	AER (box)	Rao Kotamarthi	(rao@aer.com)
G	Harvard	Larry Horowitz	(lwh@hera.harvard.edu)
H	NASA Ames	Bob Chatfield	(chatfield@clio.arc.nasa.gov)
I	NYU-Albany	Shengxin Jin	(jin@mayfly.asrc.albany.edu)
J	Jülich	Michael Kuhn	(ICH304@zam001.zam.kfa-juelich.de)
K	GFDL	Lori Perliski	(lmp@gfdl.gov)
L	Ga. Tech.	Prasad Kasibhatla	(psk@gfdl.gov)
M&	U. Camb/2-D	Kathy Law	(kathy@atm.ch.cam.ac.uk)
N	U. Camb (box)	Oliver Wild	(oliver@atm.ch.cam.ac.uk)
O&	LLNL/2-D	Doug Kinnison	(dkin@cal-bears.llnl.gov
P	LLNL/3-D	Joyce Penner	(penner1@llnl.gov)
P&	"	Cynthia Atherton	(cyndi@tropos.llnl.gov)
Q	NASA Goddard	Anne Thompson	(thompson@gator1.gsfc.nasa.gov)
R&	AER/2-D	Rao Kotomarthi	(rao@aer.com)
S	Cen. Faible Rad.	Maria Kanakidou	(mariak@asterix.saclay.cea.fr)
T	U. Oslo/3-D	Terje Berntsen	(terje.berntsen@geofysikk.uio.no)
T&	"	Ivar Isaksen	(ivar.isaksen@geofysikk.uio.no))
U	NILU	Frode Stordal	(frode@nilu.no)
Y#	U. Wash.	Hu Yang	(yang@amath.washington.edu)
Z#	Ind. Inst. Tech.	Murari Lal	(mlal@netearth.iitd.ernet.in)

Notes:
* Only a single point-of-contact is given here; for other collaborators see appropriate references.
\# Results for photolysis rates only.
& Also did delta-CH$_4$ experiment in a 2-D or 3-D model.
NYU = New York University; NILU = Norwegian Institute for Air Research

LAND, the initial NO$_x$ boosts O$_3$ levels. Over the continental boundary layer, NO$_x$ loss is rapid and the high NO$_x$ levels must be maintained by local emissions. In addition, these high-NO$_x$, ozone-producing regions have the capability of exporting significant amounts of O$_3$ (and its precursors) to the free troposphere (Pickering *et al.*, 1992; Jacob *et al.*, 1993a, b). Rapid O$_3$ formation has been observed to occur in biomass burning plumes, and the rate is predicted to depend critically on whether hydrocarbons are present (PLUME/HC) or not (PLUME/ X). In the dry upper troposphere (FREE), O$_3$ evolves very slowly, less than 1%/day, even at NO$_x$ levels of 100 ppt.

The photolysis of O$_3$ yielding O(^{1}D) is the first step in generating OH, and it controls the net production of O$_3$. Tropospheric values peak at about 4-8 km because of molecular scattering. Model predictions for this J at noon, shown in Figure 7-3a, fall within a band, ±20%

of the mean value, if a few outliers are not considered. These differences are still large considering that all models purport to be making the same calculation. Another key photolysis rate, that of NO_2 in Figure 7-3b, shows a similar range of results but with a more distinct pattern: a majority clusters within 5% of one another, and the remaining results are systematically greater or smaller by about 15%. It appears likely that this discrepancy may be caused by the different treatments of scattering, because NO_2 photolysis peaks at about 380 nm, where the only significant cause of extinction is Rayleigh scattering. It is likely that such model differences could be reduced to the 5% level with some modest effort.

The photolysis of O_3 and subsequent reaction with H_2O (reaction 2) drives the major loss of O_3 in MARINE (0 km, 10 ppt NO_x), as shown in Figure 7-3c. The spread in results after 5 days, 21 to 23 ppb, or ±12% in O_3 loss, does not seem to correlate with the O_3 photolysis rates in Figure 7-3a. Also shown in Figure 7-3c is the evolution of O_3 in LAND (0 km, 200 ppt NO_x). The additional NO_x boosts O_3 for a day or two and doubles the discrepancy in the modeled ozone. The disagreement here is important since most tropospheric O_3 is destroyed under these conditions in the wet, lower troposphere.

In the cold, dry upper troposphere, the net tendency of O_3 is for slow loss, even with initially 100 ppt of NO_x, as shown for FREE in Figure 7-3d. The divergence of results is disturbing but limited to a few models (i.e., losses after 5 days range from 2 to 4 ppb). These differences are not likely to affect the ozone budget for the majority of models. In contrast, the production of O_3 in a NO_x-rich PLUME (4 km, 10 ppb NO_x) without non-methane hydrocarbons is rapid and continues over 5 days, as shown in Figure 7-3e. Model agreement is excellent on the initial increases from 30 to 60 ppb O_3 in 48 hours, but starts to diverge as NO_x levels fall. When large amounts of NMHC are included in PLUME+HC (also Figure 7-3e), ozone is produced and NO_x depleted rapidly, in less than one day. Differences among models become much greater, in part because different chemical mechanisms for NMHC oxidation were used. (The reaction pathways and rate coefficients for chemistry with CH_4 as the only hydrocarbon have become standardized, but different approaches are used for non-methane hydrocarbons.) Some of these differences become even more obvious in the NO_x predicted for PLUME+HC as shown in Figure 7-3f. By day 3, NO_x levels in individual

models are nearly constant but with a large range, from 0 to 50 ppt.

The 24-hour averaged OH concentrations are shown for LAND and MARINE in Figure 7-3g. Values are high for LAND during the first day and demonstrate the dependence of OH on NO_x, which begins at 200 ppt and decays rapidly to about 10 ppt by day 4. The divergence among LAND results is greater than MARINE, in part due to the larger differences in the residual NO_x left from the initial value. Modeled OH values generally fall within a ±20% band. This variation in OH between models, however, does not correlate obviously as expected with any other model differences such as the photolysis rate of O_3 or the abundance of NO_x.

While O_3 and OH may seem only moderately sensitive to numerical treatment of the photochemistry, some minor species appear to be less constrained. The MARINE results for noontime formaldehyde (CH_2O), shown in Figure 7-3h, reach an approximate steady state by day 5, but the range in model results is large, about a factor of 2.

These results show that basic model-to-model differences of 30% or more exist in the calculations of O_3 change and OH concentrations. This spread is not a true scientific uncertainty, but presumably a result of different numerical methods that could be resolved given some effort, although no single fix, such as O_3 photolysis rates, would appear to reduce the spread. A more significant uncertainty in the current calculations of O_3 tendencies is highlighted by the parallel experiments with and without NMHC: the sources, transport and oxidation, and in particular the correlation of NO_x emissions and NMHC emissions on a fine scale, may control the rate at which NO_x produces O_3.

7.5.2 Intercomparison of Transport: A Case Study of Radon

A critical element in calculating tropospheric ozone is the transport of short-lived tracers such as NO_x and O_3. The model comparison that tested atmospheric transport was carried out primarily as a WCRP Workshop on short-range transport of greenhouse gases as a follow up to a similar workshop on long-range transport of CFC-11 (December 1991). A detailed description is being prepared as a WCRP Report. The basic intercomparison examined the global distribution and variability predicted for [222]Rn emitted ubiquitously by decay of ra-
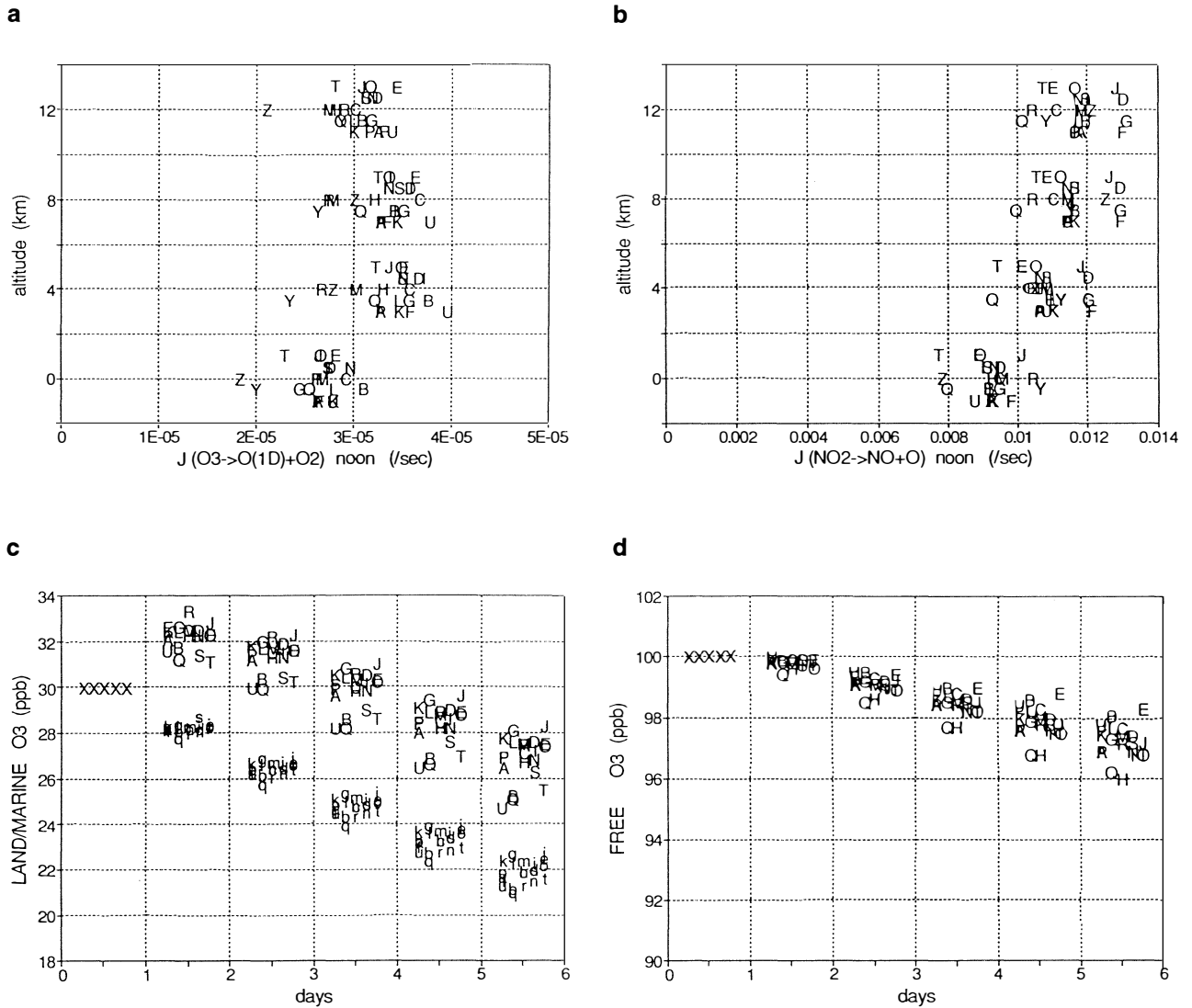
a

b

c

d

Figure 7-3. Results from the PhotoComp model intercomparison of 23 models (2 with only J-values); see Table 7-4 for the key letters and Table 7-3 for the initial conditions. Photolysis (J) rates for O_3 to $O(^1D)$ (a) and for NO_2 (b) are for local noon, July 1, 45°N, U.S. Standard Atmosphere. Results are reported for altitudes of 0, 4, 8, and 12 km. For clarity, the letter codes have been offset in altitude here, and in time-of-day in subsequent panels. Ozone mixing ratios are shown for noon in the boundary layer LAND (c, upper case codes) and MARINE (c, lower case) cases, for the FREE troposphere (d) case, and finally for the biomass
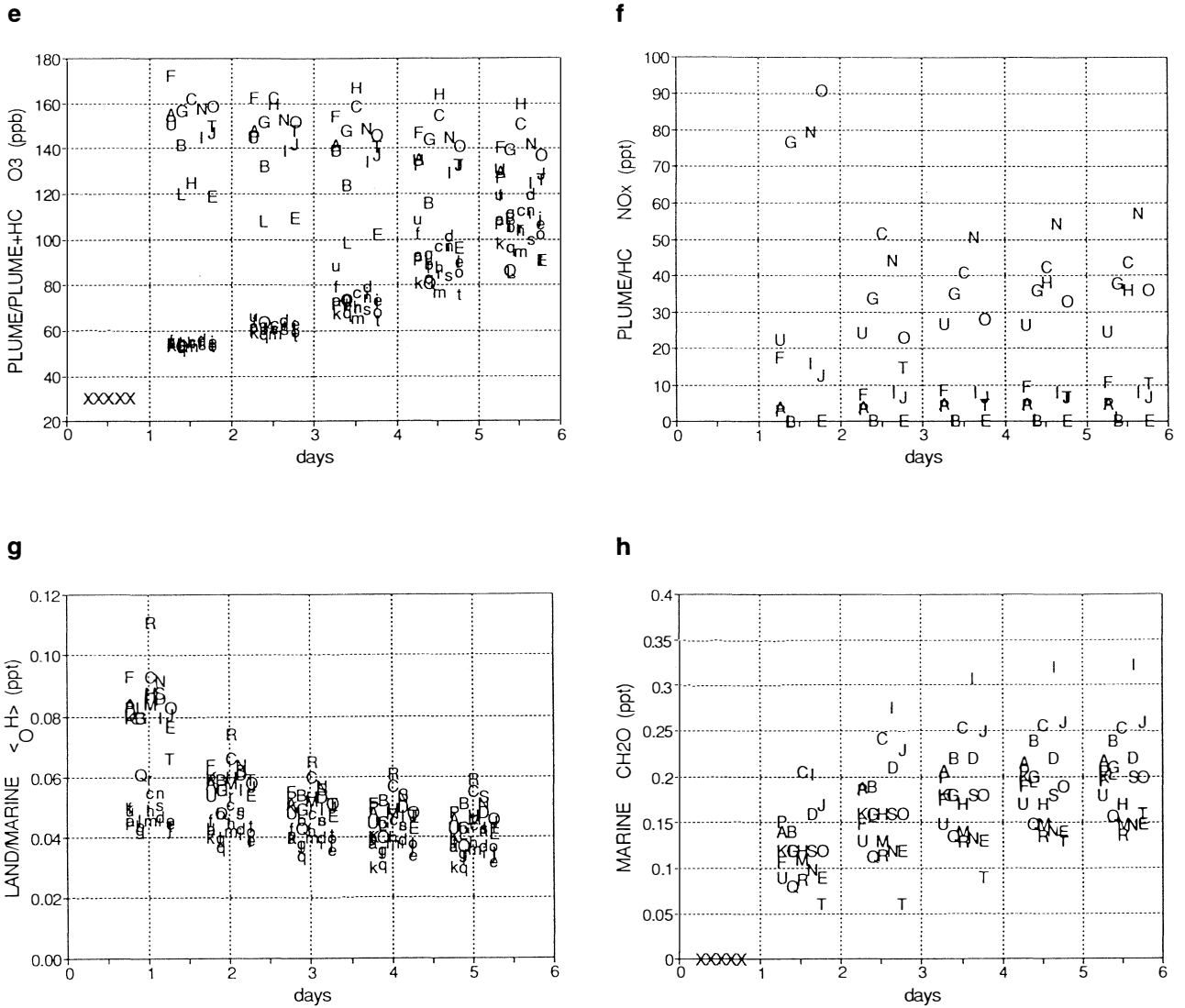
e

f

g

h

Figure 7-3, continued.
burning PLUME, without (e, lower case codes) and with NMHC (e, upper case). O_3 was initialized at the 'X'. Noontime NO_x mixing ratios are shown for the PLUME case with NMHC (f); whereas 24-hour average values of OH (from noon to noon) are shown for the 5-day integration of LAND (g). Noontime mixing ratios for CH_2O are finally given for the MARINE case (h).

Table 7-5. Models participating in the Rn/Pb transport intercomparison.

	Model	Code	Contributor
CTMs established: 3-D synoptic			
	CCM2	1	Rasch
	ECHAM3	2	Feichter/Koehler
	GFDL	3	Kasibhatla
	GISS/H/I	4	Jacob/Prather
	KNMI	5	Verver
	LLNL/Lagrange	6	Penner/Dignon
	LLNL/Euler	7	Bergman
	LMD	8	Genthon/Balkanski
	TM2/Z	9	Ramone/Balkanski/Monfray
CTMs under development: 3-D synoptic			
	CCC	10	Beagley
	LaRC	11	Grose
	LLNL/Impact	12	Rotman
	MRI	13	Chiba
	TOMCAT	14	Chipperfield
	UGAMP	15	P. Brown
CTMs used in assessments: 3-D/2-D monthly average			
	Moguntia/3-D	16	Zimmermann/Feichter
	AER/2-D	17	Shia
	UCamb/2-D	18	Law
	Harwell/2-D	19	Reeves
	UWash/2-D	20	M. Brown

KNMI = Koninklijk Nederlands Meteorologisch Instituut; LaRC = NASA Langley Research Center

dium in soils. The radon is treated as an ideal gas with constant residence time of 5.5 days. Although NO_x would seem a more relevant choice for these model comparisons, the large variations in the residence time for NO_x (*e.g.*, <1 day in the boundary layer and 10 days in the upper troposphere) make it difficult to prescribe a meaningful experiment without running realistic chemistry, a task beyond the capability of most of the participating models. Furthermore, the nonlinearity of the NO_x-OH chemistry would require that all major sources be included (see Chapter 5), which again is too difficult for this model comparison.

Twenty atmospheric models (both 3-D and 2-D) participated in the radon/lead intercomparison for CTMs (see Table 7-5). Most of the participants were using established (*i.e.*, published), synoptically varying (*i.e.*, with daily weather) 3-D CTMs; several presented results from new models under development. Among these synoptic CTMs, the circulation patterns represented the entire range: grid-point and spectral, first generation climate models (*e.g.*, GFDL and GISS), newly developed climate models (*e.g.*, CCM2 and ECHAM3), and analyzed wind fields from ECMWF (European Centre for Medium-Range Weather Forecasts) (*e.g.*, TM2Z and KNMI). One monthly averaged 3-D CTM and four longitudinally and monthly averaged 2-D models also participated.

We have a limited record of measurements of ^{222}Rn with which to test the model simulations. Some of these data are for the surface above the continental sources (*e.g.*, Cincinnati, Ohio), and some are from islands far from land sources (*e.g.*, Crozet I.). The former

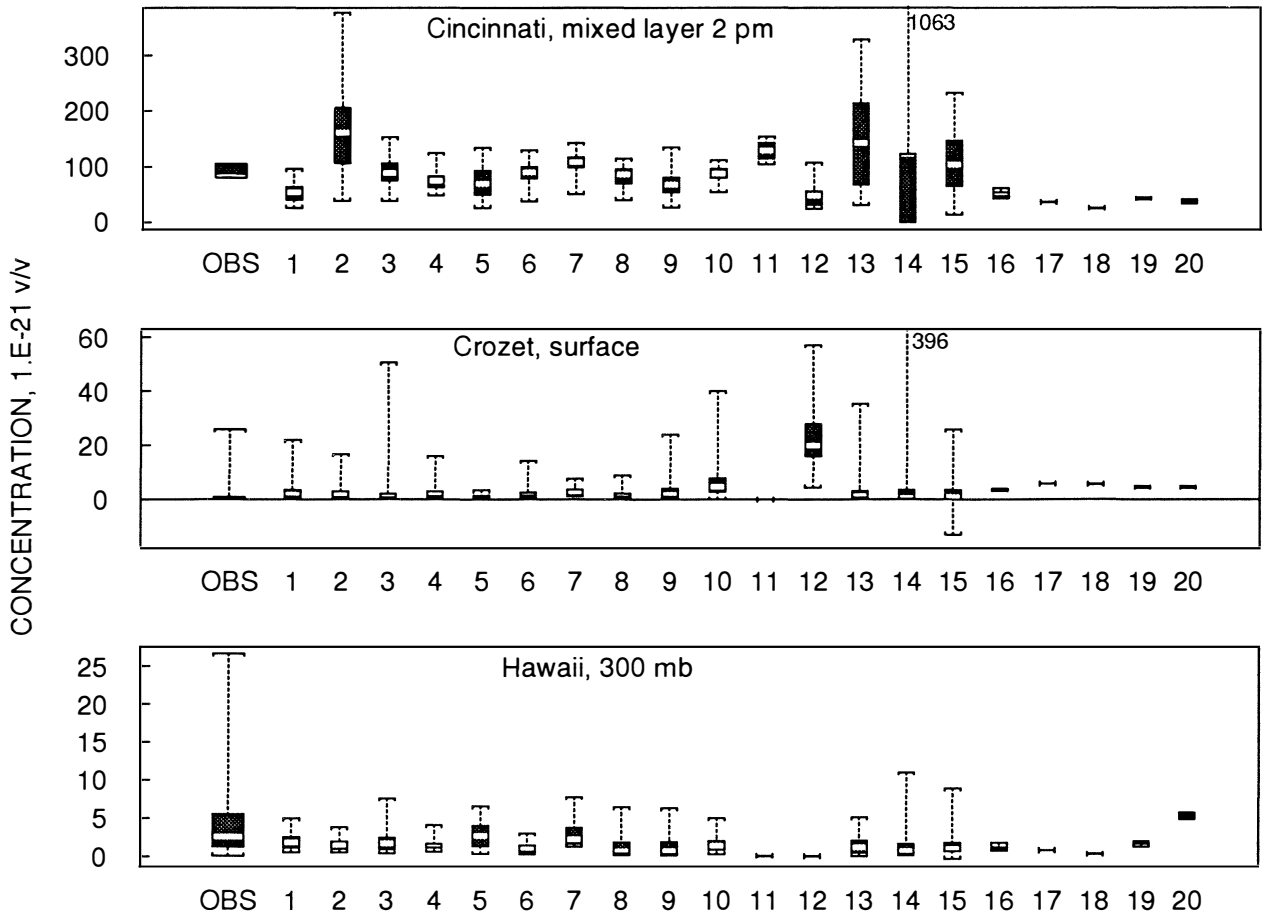RADON-222 STATISTICS FOR JUN-AUG; MODELS (CASE A) AND OBSERVATIONS

Figure 7-4. Radon-222 concentration statistics for Jun-Jul-Aug at Cincinnati, Ohio (40N 84W, mixed layer at 2 p.m.), Crozet I, (46S 51E, surface), and over Hawaii (20N 155W, 300 mbar). Modeled time series show minima and maxima, quartiles (shaded box), and medians (white band). Identification codes are given in Table 7-5. Observations at Hawaii (Balkanski *et al.*, 1992) show the same statistics; but for Cincinnati (Gold *et al.*, 1964) the shaded box gives the interannual range of June-August means; and for Crozet (Polian *et al.*, 1986) the shaded box gives typical background concentrations with the top of the vertical bar, a typical summer maximum.

sites show a diurnal cycle, with large values at the surface at night when vertical mixing is suppressed. The latter sites show a very low-level background, with large events lasting as long as a few days. An even more limited set of observations from aircraft over the Pacific (*e.g.*, 300 mbar over Hawaii) shows large variations with small layers containing very high levels of radon, obviously of recent continental origin. A set of box plots in Figure 7-4 summarizes the observations of radon at each of these three sites and compares with model predictions

(see Table 7-5 for model codes). At Cincinnati, the synoptic 3-D CTMs generally reproduce the mean afternoon concentrations in the boundary layer, although some have clear problems with excessive variability, possibly with sampling the boundary layer in the afternoon. At Crozet, most of the synoptic models can reproduce the low background with occasional radon "storms." In the upper troposphere over Hawaii, the one set of aircraft observations shows occasional, extremely high values, unmatched by any model; but the median

value is successfully simulated by several of the synoptic 3-D CTMs. The monthly averaged models could not, of course, simulate any of the time-varying observations.

The remarkable similarity of results from the synoptic CTMs for the free-tropospheric concentrations of Rn in all three experiments was a surprise to most participants. All of the established CTMs produced patterns and amplitudes that agreed within a factor of two over a dynamic range of more than 100. As an example, the zonal mean Rn from case (i) for Dec-Jan-Feb is shown for the CCM2 and ECHAM3 models in Figure 7-5a-b. The two toothlike structures result from major tropical convergence and convective uplift south of the equator and the uplift over the Sahara in the north. This basic pattern is reproduced by all the other synoptic CTMs. In Jun-Jul-Aug (not shown) the 5-contour shifts north of the equator, and again, the models produce similar patterns. In contrast, the 2-D model results, shown for the AER model in Figure 7-5c, have much smoother latitudinal structures, do not show the same seasonality, and, of course, cannot predict the large longitudinal gradients expected for Rn (similar arguments hold for NO_x; see Kanakidou and Crutzen, 1993). Results from the Moguntia CTM (monthly average 3-D winds) fell in between these two extremes and could not represent much of the structures and variations predicted by the synoptic CTMs.

Such differences in transport are critical to this assessment. Both NO_x and O_3 in the upper troposphere have chemical time scales comparable to the rate of vertical mixing, and the stratified layering seen in the monthly averaged models is likely to distort the importance of the relatively slow chemistry near the tropopause. Compared with the synoptic models, it is also obvious that the monthly averaged models would transport surface-emitted NO_x into the free troposphere very differently, which may lead to inaccurate simulation of total NO_x concentrations. The 2-D models appear to have a clear systematic bias favoring high-altitude sources (*e.g.*, stratosphere and aircraft) over surface sources (*e.g.*, combustion) and may also calculate a very different ozone response to the same NO_x perturbations.

The participating synoptic CTMs are derived from such a diverse range of circulation patterns and tracer models that the universal agreement is not likely to be fortuitous. It is unfortunate that we lack the observations to test these predictions. Nevertheless, it is clear that the

currently tested 2-D models, and to a much lesser extent the monthly averaged 3-D models, have a fundamental flaw in transporting tracers predominantly by diffusion, and they cannot simulate the global distribution of short-lived species accurately. The currently tested synoptic 3-D CTMs are the only models that have the capability of simulating the global-scale transport of NO_x and O_3; however, this capability will not be realized until these models include better simulations of the boundary layer, clouds, and chemical processes.

7.5.3 Assessing the Impact of Methane Increases

The impacts of methane perturbations are felt throughout all of atmospheric chemistry from the surface to the exosphere, and most of these mechanisms are well understood. Quantification of these effects, however, is one of the classic problems in modeling atmospheric chemistry. Similar to the ozone studies noted above, the published methane-change studies have examined scenarios that range from 700 ppb (pre-industrial) to 1700 ppb (current) to a doubling by the year 2050 (*e.g.*, WMO, 1992), but these scenarios are not consistent across models. This delta-CH_4 study was designed to provide a common framework for evaluating the multitude of indirect effects, especially changes in O_3 and OH, that are associated with an increase in CH_4. The study centers on today's atmosphere: use each model's best simulation of the current atmosphere and then increase the CH_4 concentration (not fluxes) in the troposphere by 20%, from 1715 ppb to 2058 ppb (expected in about 30 years based on observed 1980-1990 trend). This increase is small enough so that perturbations to current atmospheric chemistry should be approximately linear. The history and protocol of the delta-CH_4 assessment is the same as that of PhotoComp described above, and the six participating research groups are also denoted in Table 7-4.

THE CURRENT ATMOSPHERE

Important diagnostics from delta-CH_4 include O_3 and NO_x profiles for the current atmosphere, providing a test of the realism of each model's simulation. Typical profiles observed for O_3 in the tropics and in northern midlatitudes over America and Europe are shown in Figure 7-6. The corresponding calculated O_3 profiles,

Figure 7-5. Latitude by altitude contours of chemical transport model simulations of a continental source of radon-222. Units are 1E-21 v/v. Zonal means for the period Dec-Jan-Feb are shown for two 3-D models, (a) CCM2 and (b) ECHAM3, and for (c) the AER 2-D model. These results are examples form a WCRP workshop on tracer transport.
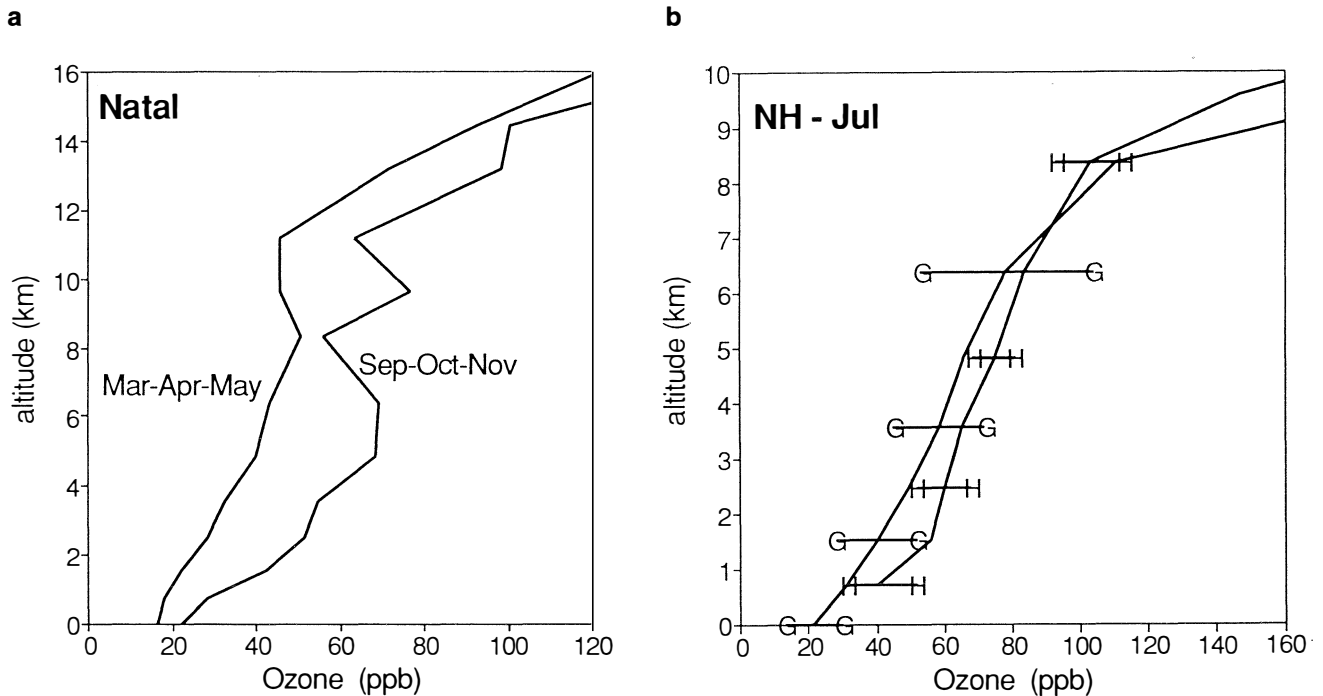
a

b

Figure 7-6. Observed mean profiles of O_3 in the tropics (Natal, panel a) and at northern midlatitudes in July (G = Goose Bay and H = Hohenpeissenberg, panel b). Data from northern stations were averaged over 1980-1991. Tropical station shows seasons of minimum (Mar-Apr-May) and maximum (Sep-Oct-Nov) ozone. Source: Logan, 1994; Kirchhoff *et al.*, 1990.

shown in Figure 7-7a-b, differ by almost a factor of two, but encompass the observations. Clear divergence of results above 10 km altitude illustrates difficulties in determining the transition between troposphere and stratosphere. This exercise is only the beginning of an objective evaluation of tropospheric ozone models through comparison with measurements.

The modeled zonal-mean NO_x profiles, shown in Figure 7-7c, differ by up to almost a factor of 10. Comparisons in the lowest 2 km altitude are not meaningful since the CTMs average regions of high urban pollution with clean marine boundary layer. The range of modeled NO_x values in the free troposphere often falls outside the range of typical observations, about 20 to 100 ppt (see Chapter 5).

O_3 PERTURBATIONS

The predicted changes in tropospheric O_3 for Jun-Jul-Aug in northern midlatitudes and the tropics are shown in Figure 7-8a and 7-8b for the delta-CH_4 study.

Ozone increases everywhere in the troposphere, by values ranging from about 0.5 ppb to more than 5 ppb. (The extremely high values for model P in the upper troposphere must be considered cautiously since this recent submission has not yet been scrutinized as much as the other results.) In general the increase is larger at midlatitudes, but not for all models. Results for the southern midlatitudes in summer (Dec-Jan-Feb) (not shown) are similar to the northern.

The large spread in these results shows that our ability to predict changes in tropospheric O_3 induced by CH_4 perturbations is not very good. This conclusion is not unexpected given the large range in modeled NO_x (Figure 7-7c), but the differences in O_3 perturbations do not seem to correlate with the NO_x distribution in the models. Nevertheless, a consistent pattern of increases in tropospheric O_3, ranging from 0.5 to 2.5 ppb, occurs throughout most of the troposphere. Our best estimate is that a 20% increase in CH_4 would lead to an increase in ozone of about 1.5 ppb throughout most of the tropo-
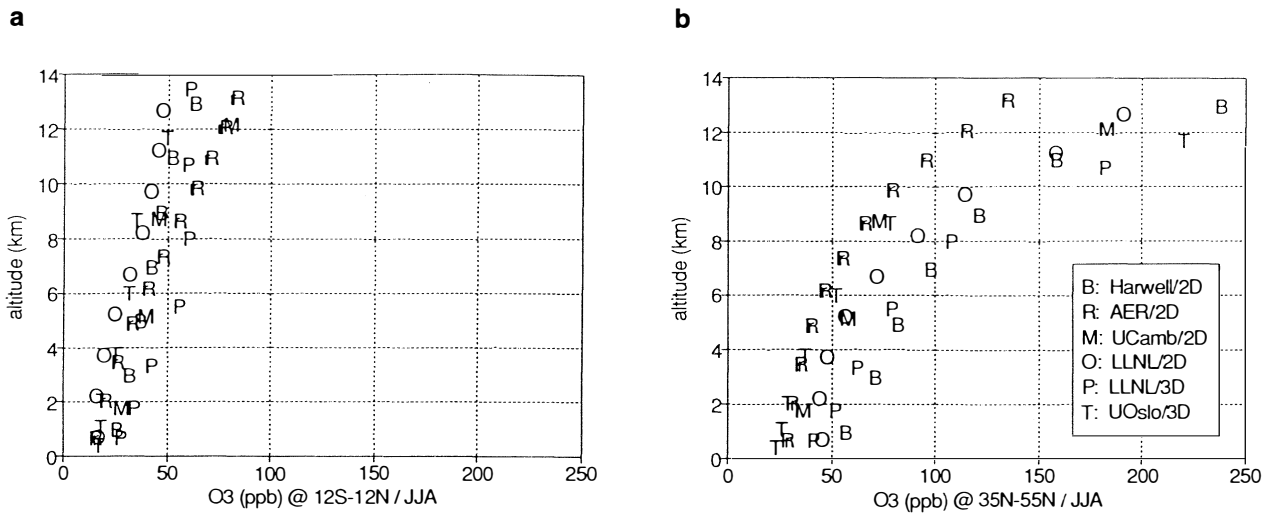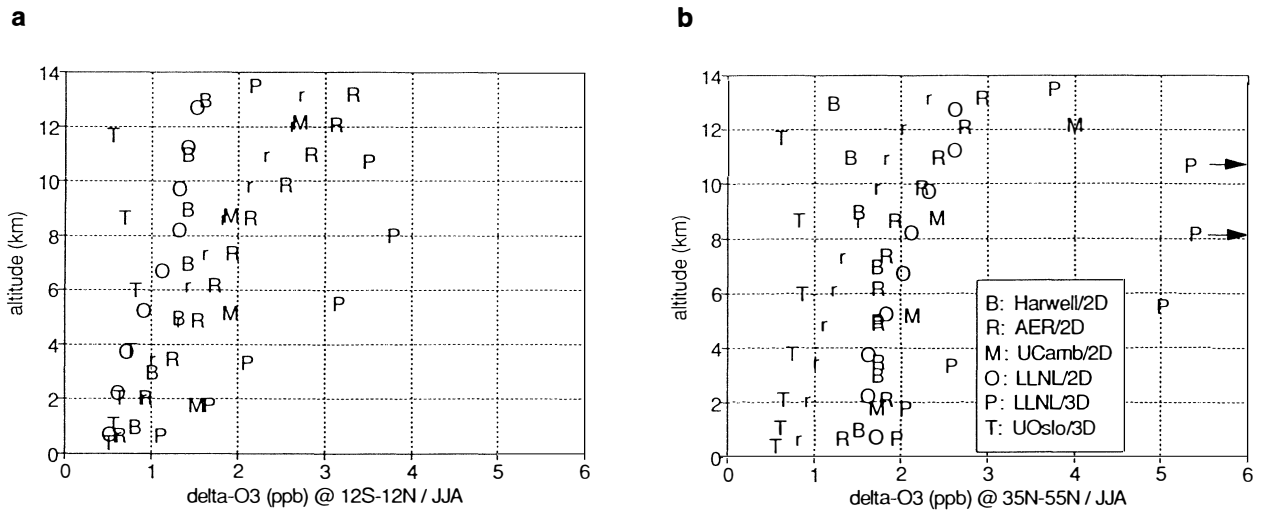
a

b

Figure 7-7. Modeled tropospheric O_3 (panel a: 12S-12N, b: 35N-55N) and NO_x (c: 35N-55N) for the current atmosphere averaged over Jun-Jul-Aug. For key, see Table 7-4.

c

Figure 7-8. (Below). Modeled change in O_3 for a 20% increase in CH_4, averaged over Jun-Jul-Aug (panel a: 12S-12N, b: 35N-55N). For key, see Table 7-4.

a

b

Table 7-6. Inferred CH_4 response time from delta-CH_4 simulations.

Model code	FF*	RT/LT**
B	-0.20%	1.29
M	-0.17%	1.23#
O	-0.35%	1.62
P	-0.22%	1.32
R	-0.26%	1.39
(R)	-0.18%	1.26#
T	-0.34%	1.61

Notes:

* FF = feedback factor, relative change (%) in the globally averaged CH_4 loss frequency (*i.e.*, (OH)) for a +1% increase in CH_4 concentrations

** RT = residence time and LT = lifetime

\# Uses fixed CO concentrations, underestimates this ratio.

sphere in both tropics and summertime midlatitudes. This indirect impact on the radiative forcing is about 25% ± 15% of that due to the 343 ppb increase in CH_4 alone.

RESIDENCE TIME OF CH_4 EMISSIONS

Methane is the only long-lived gas that has a clearly identified, important chemical feedback: increases in atmospheric CH_4 reduce tropospheric OH, increase the CH_4 lifetime, and hence amplify the climatic and chemical impacts of a CH_4 perturbation (Isaksen and Hov, 1987; Berntsen *et al.*, 1992). The delta-CH_4 simulations from six different 2-D and 3-D models show that these chemical feedbacks change the relative loss rate for CH_4 by -0.17% to -0.35% for each 1% increase in CH_4 concentration, as shown in Table 7-6. This range can reflect differences in the modeled roles of CH_4, CO, and NMHC as sinks for OH (Prather, 1994). For example, model M, with the smallest feedback factor, has fixed the concentrations of CO; and model R has shown that calculating CO instead with a flux boundary condition (as most of the other models have done) results in a larger feedback. These differences cannot be resolved with this intercomparison, and this range underestimates our uncertainty in this factor.

Recent theoretical analysis has shown that the feedback factor (FF) defined in Table 7-6 can be used to derive a residence time that accurately describes the time scale for decay of a pulse of CH_4 added to the atmosphere. Effectively, a pulse of CH_4, no matter how small, reduces the global OH levels by a similar amount (*i.e.*, -0.3% per +1%). This leads to the buildup of a corresponding increase in the already-existing atmospheric reservoir of CH_4, that, in net, cannot be distinguished from a longer residence time for the initial pulse. Thus the residence time (RT) is longer than the lifetime (LT) derived from the budget (*i.e.*, total abundance divided by total losses). Prather (1994) has shown that the ratio, RT/LT, is equal to $1/(1 + FF)$ and that this residence time applies to all CH_4 perturbations, positive or "negative," no matter how small or large, as long as the change in CH_4 concentration is not so large as to change the feedback factor. Based on model results, this assumption should apply at least over a ±30% change in current CH_4 concentrations. Two of the models with results in Table 7-6 have shown that small CH_4 perturbations decay with the predicted residence time.

Based on these limited results, we choose 1.45 as the best guess for the ratio RT/LT, with an uncertainty bracket of 1.20 to 1.70. The budget lifetime of CH_4 is calculated to be about 9.4 yr, using the CH_3CCl_3 lifetime as a standard for OH and including stratospheric and soil losses. Thus, the residence time for any additional emissions of CH_4 is 13.6 yr (11.3-16.0 yr). This enhanced time scale describes the effective duration for all current

emissions of CH_4; it is independent of other emissions as long as current concentrations of CH_4, within ±30%, are maintained. Some of this effect was included in the previous assessment as an "indirect OH" enhancement to the size of the CH_4 perturbations. Here we recognize that the OH chemical feedback gives a residence time for CH_4 emissions that is substantially longer than the lifetime used to derive the global budgets. This effective lengthening of a CH_4 pulse applies also to all induced chemical perturbations such as tropospheric O_3 and stratospheric H_2O.

REFERENCES

Balkanski, Y.J., and D.J. Jacob, Transport of continental air to the subantarctic Indian Ocean, *Tellus, 42B,* 62–75, 1990.

Balkanski, Y.J., D.J. Jacob, R. Arimoto, and M.A. Kritz, Long-range transport of radon-222 over the North Pacific Ocean: Implications for continental influences, *J. Atmos. Chem., 14,* 353–374, 1992.

Balkanski, Y.J., D.J. Jacob, G.M. Gardner, W.M. Graustein, and K.K. Turekian, Transport and residence times of continental aerosols inferred from a global 3-dimensional simulation of ^{210}Pb, *J. Geophys. Res., 98,* 20573–20586, 1993.

Berntsen, T., J.S. Fuglestvedt, and I.S.A. Isaksen, Chemical-dynamical modelling of the atmosphere with emphasis on the methane oxidation, *Ber. Bunsenges. Phys. Chem., 96,* 3, 241–251, 1992.

Berntsen, T.K., and I.S.A. Isaksen, A 3-D photochemistry/transport model of the global troposphere, Report No. 89, Institute for Geophysics, University of Oslo, Norway, 1994.

Brost, R.A., J. Feichter, and M. Heimann, Three-dimensional simulation of ^7Be in a global climate model, *J. Geophys. Res., 96,* 22423–22445, 1991.

Brühl, C., and P.J. Crutzen, On the disproportionate role of tropospheric ozone as a filter against solar UV-B radiation, *Geophys. Res. Lett., 17,* 703–706, 1989.

Chameides, W.L., P.S. Kasibhatla, J.J. Yienger, H. Levy II, and W.J. Moxim, The growth of continental-scale metro-agro-plexes, regional ozone pollution, and world food production, *Science, 264,* 74–77, 1994.

Chatfield, R.B., The anomalous HNO_3/NO_x ratio of remote tropospheric air: Is there conversion of nitric acid to formic acid and NO_x?, submitted to *Geophys. Res. Lett.,* 1994.

Chin, M., D.J. Jacob, J.W. Munger, D.D. Parrish, and B.G. Doddridge, Relationship of ozone and carbon monoxide over North America, *J. Geophys. Res., 99,* 14565–14573, 1994.

Crutzen, P.J., and P.H. Zimmermann, The changing photochemistry of the troposphere, *Tellus, 43AB,* 136–151, 1991.

Danielsen, E.F., and V. Mohnen, Project Duststorm: Ozone transport, in situ measurements, and meteorological analysis of tropopause folding, *J. Geophys. Res., 82,* 5867–5877, 1977.

Derwent, R.G., The influence of human activities on the distribution of hydroxyl radicals in the troposphere, submitted to *Philosophical Transactions of the Royal Society,* 1994.

Easter, R.C., R.D. Saylor, and E.G. Chapman, Analysis of mid-tropospheric carbon monoxide data using a three-dimensional global atmospheric chemistry numerical model, in *Proceedings 20th Inter. Tech. Meeting on Air Pollution Modeling and Its Application,* Valencia, Spain, 1993.

Fan, S.-M., D.J. Jacob, D.L. Mauzerall, J.D. Bradshaw, S.T. Sandholm, D.R. Blake, H.B. Singh, R.W. Talbot, G.L. Gregory, and G.W. Sachse, Origin of tropospheric NO_x over subarctic eastern Canada in summer, *J. Geophys. Res., 99,* 16867-16877, 1994.

Feichter, J., and P.J. Crutzen, Parameterization of vertical tracer transport due to deep cumulus convection in a global transport model and its evaluation with $^{222}Radon$ measurements, *Tellus, 42B,* 100–117, 1990.

Feichter, J., R.A. Brost, and M. Heimann, Three-dimensional modeling of the concentration and deposition of ^{210}Pb aerosols, *J. Geophys. Res., 96,* 22447–22460, 1991.

Flatøy, F., *Modelling of Coupled Physical and Chemical Processes in the Troposphere over Europe,* Ph.D. Thesis, Geophysical Institute, University of Bergen, Norway, 1994.

Flatøy, F., Ø. Hov, and H. Smit, 3-D model studies of vertical exchange processes in the troposphere over Europe, submitted to *J. Geophys. Res.,* 1994.

Fuglestvedt, J.S., J.E. Jonson, and I.S.A. Isaksen, Effects of reductions in stratospheric ozone on tropospheric chemistry through changes in photolysis rates, *Tellus, 46B,* 172–192, 1994a.

Fuglestvedt, J.S., J.E. Jonson, W.-C. Wang, and I.S.A. Isaksen, Responses in tropospheric chemistry to changes in UV fluxes, temperatures and water vapour densities, to appear in *Atmospheric Ozone as a Climate Gas*, edited by W.-C. Wang and I.S.A. Isaksen, NASA ASI Series, in press, 1994b.

Fung, I., J. John, J. Lerner, E. Matthews, M. Prather, L.P. Steele, and P.J. Fraser, Three-dimensional model synthesis of the global methane cycle, *J. Geophys. Res., 96,* 13033–13066, 1991.

Gallardo, L., H. Rodhe, and P.J. Crutzen, Evaluation of a global 3-D model of the tropospheric reactive nitrogen cycle, submitted to *J. Geophys. Res.,* 1994.

Galloway, J.N., H. Levy II, and P.S. Kasibhatla, Year 2020: Consequences of population growth and development on deposition of oxidized nitrogen, *Ambio, 23,* 120–123, 1994.

Gidel, L.T., and M.A. Shapiro, General circulation estimates of the net vertical flux of ozone in the lower stratosphere and the implications for the tropospheric ozone budget, *J. Geophys. Res., 85,* 4049–4058, 1980.

Gleason, J.F., P.K. Bhartia, J.R. Herman, R. McPeters, P. Newman, R.S. Stolarski, L. Flynn, G. Labow, D. Larko, C. Seftor, C. Wellemeyer, W.D. Komhyr, A.J. Miller, and W. Planet, Record low global ozone in 1992, *Science, 260,* 523–526, 1993.

Gold, S., H. Barkhau, W. Shleien, and B. Kahn, Measurement of naturally occurring radionuclides in air, in *The Natural Radiation Environment*, edited by J.A.S. Adams and W.M. Lowder, University of Chicago Press, 369–382, 1964.

Hauglustaine, D.A., C. Granier, G.P. Brasseur, and G. Mégie, The importance of atmospheric chemistry in the calculation of radiative forcing on the climate system, *J. Geophys. Res., 99,* 1173–1186, 1994.

IPCC, Intergovernmental Panel on Climate Change, *Radiative Forcing of Climate Change,* The 1994 Report of the Scientific Assessment Working Group of IPCC, 1994.

Isaksen, I.S.A., and Ø. Hov, Calculation of trends in the tropospheric concentration of O_3, OH, CH_4, and NO_x, *Tellus, 39B,* 271–285, 1987.

Jacob, D.J., M.J. Prather, S.C. Wofsy, and M.B. McElroy, Atmospheric distribution of [85]Kr simulated with a general circulation model, *J. Geophys. Res., 92,* 6614–6626, 1987.

Jacob, D.J., and M.J. Prather, Radon-222 as a test of convection in a general circulation model, *Tellus, 42,* 118–134, 1990.

Jacob, D.J., S.C. Wofsy, P.S. Bakwin, S.-M. Fan, R.C. Harriss, R.W. Talbot, J.D. Bradshaw, S.T. Sandholm, H.B. Singh, E.V. Browell, G.L. Gregory, G.W. Sachse, M.C. Shipham, D.R. Blake, and D.R. Fitzjarrald, Summertime photochemistry of the troposphere at high northern latitudes, *J. Geophys. Res., 97,* 16421–16431, 1992.

Jacob, D.J., J.A. Logan, R.M. Yevich, G.M. Gardner, C.M. Spivakovsky, S.C. Wofsy, J.W. Munger, S. Sillman, M.J. Prather, M.O. Rodgers, H. Westberg, and P.R. Zimmerman, Simulation of summertime ozone over North America, *J. Geophys. Res., 98,* 14797–14816, 1993a.

Jacob, D.J., J.A. Logan, G.M. Gardner, R.M. Yevich, C.M. Spivakovsky, S.C. Wofsy, S. Sillman, and M.J. Prather, Factors regulating ozone over the United States and its export to the global atmosphere, *J. Geophys. Res., 98,* 14817–14826, 1993b.

Johnson, C.E., The sensitivity of a two-dimensional model of global tropospheric chemistry to emissions at different latitudes, *AEA Environment & Energy,* United Kingdom Atomic Energy Authority, AEA-EE-0407, 1993.

Johnson, C., J. Henshaw, and G. McInnes, Impact of aircraft and surface emissions of nitrogen oxides on tropospheric ozone and global warming, *Nature, 355,* 69-71, 1992.

Kanakidou, M., and P.J. Crutzen, Scale problems in global tropospheric chemistry modelling: Comparison of results obtained with a three-dimensional model, adopting longitudinally uniform and varying emissions of NO_x and NMHC, *Chemosphere, 26* (1-4), 787–801, 1993.

Kanakidou, M., H.B. Singh, K.M. Valentin, and P.J. Crutzen, A two-dimensional model study of ethane and propane oxidation in the troposphere, *J. Geophys. Res., 96,* 15395-15413, 1991.

Kanakidou, M., P.J. Crutzen, P.H. Zimmermann, and B. Bonsang, A 3-dimensional global study of the photochemistry of ethane and propane in the troposphere: Production and transport of organic nitrogen compounds, in *Air Pollution Modelling and Its Application IX,* edited by H. van Dop and G. Kallos, Plenum Press, New York, 415–426, 1992.

Kasibhatla, P.S., H. Levy II, W.J. Moxim, and W.L. Chameides, The relative impact of stratospheric photochemical production on tropopsheric NO_y levels: A model study, *J. Geophys. Res., 96,* 18631–18646, 1991.

Kasibhatla, P.S., NO_y from sub-sonic aircraft emissions: A global three-dimensional model study, *Geophys. Res. Lett., 20,* 1707–1710, 1993.

Kasibhatla, P.S., H. Levy II, and W.J. Moxim, Global NO_x, HNO_3, PAN, and NO_y distributions from fossil fuel combustion emissions: A model study, *J. Geophys. Res., 98,* 7165–7180, 1993.

Kaye, J., S. Penkett, and F.M. Ormond (eds.), *Concentrations, Lifetimes and Trends of CFCs, Halons, and Related Species,* National Aeronautics and Space Administration Reference Publication No. 1339, 1994.

Kerr, J.B., and C.T. McElroy, Evidence for large upward trends of ultraviolet-B radiation linked to ozone depletion, *Science, 262,* 1032–1034, 1993.

Kirchhoff, V.W.J.H., I.M.O. da Silva, and E.V. Browell, Ozone measurements in Amazonia: Dry season versus wet season, *J. Geophys. Res., 95,* 16913–16926, 1990.

Law, K.S., and J.A. Pyle, Modelling trace gas budgets in the troposphere 1. Ozone and odd nitrogen, *J. Geophys. Res., 98,* 18377–18400, 1993a.

Law, K.S., and J.A. Pyle, Modelling trace gas budgets in the troposphere 2. CH_4 and CO, *J. Geophys. Res., 98,* 18401–18412, 1993b.

Lelieveld, J., Model simulations of the 1850 and 1990 atmosphere chemical compositions, accepted for publication in *J. Geophys. Res.,* 1994.

Lelieveld, J., and P. Crutzen, Role of deep convection in the ozone budget of the troposphere, *Science, 264,* 1759–1761, 1994.

Liu, S.C., and M. Trainer, Responses of tropospheric ozone and odd hydrogen radicals to column ozone change, *J. Atmos. Chem., 6,* 221–233, 1988.

Liu, S.C., S.A. McKeen, and S. Madronich, Effect of anthropogenic aerosols on biologically active ultraviolet radiation, *Geophys. Res. Lett., 18,* 2265–2268, 1991.

Logan, J.A., Trends in the vertical distribution of ozone: An analysis of ozonesonde data, submitted to *J. Geophys. Res.,* 1994.

Madronich, S., and C. Granier, Impact of recent total ozone changes on tropospheric ozone photodissociation, hydroxyl radicals, and methane trends, *Geophys. Res. Lett., 19,* 465–467, 1992.

Mahlman, J.D., H. Levy II, and W.J. Moxim, Three-dimensional tracer structure and behavior as simulated in two ozone precursor experiments, *J. Atmos. Sci., 37,* 655–685, 1980.

Montzka, S.A., R.C. Myers, J.H. Butler, and J.W. Elkins, Global tropospheric distribution and calibration scale of HCFC-22, *Geophys. Res. Lett., 20,* 703–706, 1993.

Murphy, D.M., D.W. Fahey, M.H. Proffitt, S.C. Liu, K.R. Chan, C.S. Eubank, S.R. Kawa, and K.K. Kelly, Reactive nitrogen and its correlation with ozone in the lower stratosphere and the upper troposphere, *J. Geophys. Res., 98,* 8751–8773, 1993.

Müller, J.-F., and G. Brasseur, IMAGES: A three-dimensional chemical transport model of the troposphere, accepted for publication in *J. Geophys. Res.,* 1994.

Patten, K.O., P.S. Connell, D.E. Kinnison, D.J. Wuebbles, L. Froidevaux, and T.G. Slanger, Effect of vibrationally excited oxygen on ozone production in the stratosphere, *J. Geophys. Res., 99,* 1211–1223, 1994.

Penner, J.E., C.S. Atherton, J. Dignon, S.J. Ghan, J.J. Walton, and S. Hameed, Tropospheric nitrogen: A three-dimensional study of sources, distributions, and deposition, *J. Geophys. Res., 96,* 959–990, 1991.

Penner, J.E., C.S. Atherton, and T.E. Graedel, Global emissions and models of photochemically active compounds, in *Global Atmospheric-Biospheric Chemistry*, edited by R. Prinn, Plenum Publ., New York, 223-248, 1994.

Pickering, K.E., A.M. Thompson, J.R. Scala, W.-K. Tao, and J. Simpson, Ozone production potential following convective redistribution of biomass burning emissions, *J. Atmos. Chem., 14,* 297–313, 1992.

Pickering, K.E., A.M. Thompson, W.-K. Tao, and T.L. Kucsera, Upper tropospheric ozone production following mesoscale convection during STEP/EMEX, *J. Geophys. Res., 98,* 8737–8749, 1993.

Polian, G., G. Lambert, B. Ardouin, and A. Jegou, Long-range transport of radon in sub-Antarctic and Antarctic areas, *Tellus, 38B,* 178–189, 1986.

Prather, M.J., Lifetimes and eigenstates in atmospheric chemistry, *Geophys. Res. Lett., 21,* 801–804, 1994.

Prather, M.J., M. McElroy, S. Wofsy, G. Russell, and D. Rind, Chemistry of the global troposphere: Fluorocarbons as tracers of air motion, *J. Geophys. Res., 92,* 6579–6613, 1987.

Prather, M.J., and E.E. Remsberg (eds.), *The Atmospheric Effects of Stratospheric Aircraft: Report of the 1992 Models and Measurements Workshop,* National Aeronautics and Space Administration Reference Publication No. 1292, 1992.

Prinn, R., D. Cunnold, P. Simmonds, F. Alyea, R. Boldi, A. Crawford, P. Fraser, D. Gutzler, D. Hartley, R. Rosen, and R. Rasmussen, Global average concentration and trend for hydroxyl radicals deduced from ALE/GAGE trichloroethane (methyl chloroform) data for 1978-1990, *J. Geophys. Res., 97,* 2445–2461, 1992.

Roemer, M.G.M., and K.D. van der Hout, Emissions of NMHCs and NO_x and global ozone production, in *Proceedings of the 19th NATO/CCMS International Technical Meeting on Air Pollution Modelling and Its Application,* North Atlantic Treaty Organization/Committee on the Challenges of Modern Society, September 29–October 4, 1991, Crete, Greece, Plenum Press, New York, 1992.

Simpson, D., Photochemical model calculations over Europe for two extended summer periods: 1985 and 1989. Model results and comparison with observations, *Atmos. Environ., 27A,* 921–943, 1993.

Singh, H.B., D. O'Hara, D. Herlth, J.D. Bradshaw, S.T. Sandholm, G.L. Gregory, G.W. Sachse, D.R. Blake, P.J. Crutzen, and M. Kanakidou, Atmospheric measurements of peroxyacetyl nitrate and other organic nitrates at high-latitudes: Possible sources and sinks, *J. Geophys. Res., 97,* 16511–16522, 1992.

Singh, H.B., and M. Kanakidou, An investigation of the atmospheric sources and sinks of methyl bromide, *Geophys. Res. Lett., 20,* 133-136, 1993.

Singh, H.B., D. O'Hara, D. Herlth, W. Sachse, D.R. Blake, J.D. Bradshaw, M. Kanakidou, and P.J. Crutzen, Acetone in the atmosphere: Distribution, sources and sinks, *J. Geophys. Res., 99,* 1805–1820, 1994.

Smith, R.C., B.B. Prézelin, K.S. Baker, R.R. Bidigare, N.P. Boucher, T. Coley, D. Karstenz, S. MacIntyre, H. Matlick, D. Menzies, M. Ondrusek, Z. Wan, and K.J. Waters, Ozone depletion: Ultraviolet radiation and phytoplankton biology in Antarctic waters, *Science, 255,* 952–959, 1992.

Spivakovsky, C.M., R. Yevich, J.A. Logan, S.C. Wofsy, M.B. McElroy, and M.J. Prather, Tropospheric OH in a three-dimensional chemical tracer model: An assessment based on observations of CH_3CCl_3, *J. Geophys. Res., 95,* 18441–18472, 1990a.

Spivakovsky, C.M., S.C. Wofsy, and M.J. Prather, A numerical method for parameterization of atmospheric chemistry: Computation of tropospheric OH, *J. Geophys. Res., 95,* 18433–18440, 1990b.

Spivakovsky, C.M., and Y.J. Balkanski, Tropospheric OH: Constraints imposed by observations of ^{14}CO and methyl chloroform, in *Report of the WMO-Sponsored Meeting of Carbon Monoxide Experts,* edited by P.C. Novelli and R.M. Rosson, Global Atmospheric Watch, World Meteorological Organization, Geneva, in press, 1994.

Strand, A., and Ø. Hov, A two-dimensional zonally averaged transport model including convective motions and a new strategy for the numerical solution, *J. Geophys. Res., 98,* 9023–9037, 1993.

Strand, A., and Ø. Hov, Two-dimensional global study of the tropospheric ozone production, accepted for publication in *J. Geophys. Res.,* 1994.

Tie, X., C.-Y. Kao, E.J. Mroz, R.J. Cicerone, F.N. Alyea, and D.M. Cunnold, Three-dimensional simulations of atmospheric methyl chloroform: Effect of an ocean sink, *J. Geophys. Res., 97,* 20751–20769, 1992.

Thompson, A.M., The oxidizing capacity of the Earth's atmosphere: Probable past and future changes, *Science, 256,* 1157–1165, 1992.

WMO, *Scientific Assessment of Ozone Depletion: 1989,* World Meteorological Organization Global Ozone Research and Monitoring Project – Report No. 20, Geneva, 1990.

WMO, *Scientific Assessment of Ozone Depletion: 1991,* World Meteorological Organization Global Ozone Research and Monitoring Project – Report No. 25, Geneva, 1992.

Wuebbles, D.J., J.S. Tamaresis, and K.O. Patten, *Quantified Estimates of Total GWPs for Greenhouse Gases Taking Into Account Tropospheric Chemistry,* Lawrence Livermore National Laboratory UCRL-115850, 1993.